Article:
Hussein, MS and Lesnic, D (2016) Simultaneous determination of time and space-dependent coefficients in a parabolic equation. Communications in Nonlinear Science and Numerical Simulation, 33. 194 - 217. ISSN: 1007-5704

https://doi.org/10.1016/j.cnsns.2015.09.008

Simultaneous determination of time and space-dependent coefficients in a parabolic equation

M.S. Hussein[1,2] and D. Lesnic[1]
[1]*Department of Applied Mathematics, University of Leeds, Leeds LS2 9JT, UK*
[2]*Department of Mathematics, College of Science, University of Baghdad, Baghdad, Iraq*
E-mails: mmmsh@leeds.ac.uk (M.S. Hussein), amt5ld@maths.leeds.ac.uk (D. Lesnic).

Abstract
This paper investigates a couple of inverse problems of simultaneously determining time and space dependent coefficients in the parabolic heat equation using initial and boundary conditions of the direct problem and overdetermination conditions. The measurement data represented by these overdetermination conditions ensure that these inverse problems have unique solutions. However, the problems are still ill-posed since small errors in the input data cause large errors in the output solution. To overcome this instability we employ the Tikhonov regularization method. The finite-difference method (FDM) is employed as a direct solver which is fed iteratively in a nonlinear minimization routine. Both exact and noisy data are inverted. Numerical results for a few benchmark test examples are presented, discussed and assessed with respect to the FDM mesh size discretisation, the level of noise with which the input data is contaminated, and the chosen regularization parameters.

Keywords: Inverse problem; Finite-difference method; Tikhonov regularization; Heat equation; Nonlinear optimization.

1 Introduction

Coefficient identification problems typically involve the estimation of certain coefficients based on inexact measurements of other measurable quantities. The estimate process is often ill-posed in the sense that small noise in the input data may lead to dramatic error in the solution. Therefore, techniques like Tikhonov regularization [24], mollification [19] and iterative regularization methods have been developed to deal with this instability, [27].

Choosing an appropriate additional information about what quantities to measure or supply is important since this data enables us to identify the unknown coefficients uniquely. For instance, an upper-base final temperature condition was chosen in [4] to identify a space-dependent heat source, and a similar version can be found in [2] where a Cauchy problem for a second-order parabolic equation was formulated for determining a space-dependent coefficient of a low-order derivative. Cauchy data have also been used in [5] for reconstructing numerically a temperature-dependent thermal conductivity or a heat source. The determination of the space-dependent thermal conductivity was studied in [20] using Kansa's method based on radial basis function techniques, and in [6] using a predictor-corrector iterative finite-difference method (FDM). While spacewise dependent perfusion coefficient identification in the transient bio-heat equation subjected to time-averaging temperature measurement was investigated in [25] using the Crank-Nicolson FDM scheme combined with the first-order Tikhonov regularization method. On the other hand, time-dependent coefficient identification problems have been investigated recently, just to mention a few, the time-dependent inverse source identification problem [7, 22, 26]

and the thermal conductivity/diffusivity identification problem [9, 17] subjected to various kinds of overdetermination conditions.

In this paper, we consider obtaining the numerical solution of a couple of related inverse time and space-dependent coefficient identification problems in the parabolic heat equation subjected to nonlocal, time-averaging overdetermination conditions.

The organisation of this paper is as follows. In Section 2, the mathematical formulations of the inverse problems are given. In Sections 3, the finite difference scheme based on the Crank-Nicholson method is developed for solving the direct problem. In Section 4, the inverse problems are reformulated as nonlinear least-squares minimization problems further penalized with Tikhonov's regularization terms in order to achive stable solutions with respect to noise in the input data. Numerical results illustrate that accurate and stable numerical solutions are obtained, as it is discussed in Section 5. Finally, the conclusions of this research are drawn in Section 6.

2 Mathematical formulation

Let $L > 0$ and $T > 0$ be fixed numbers representing the length of a one-dimensional finite slab and the time period, respectively, and denote by $Q_T := (0, L) \times (0, T)$ the solution domain. Let also f represent a given heat source. Then consider the inverse problem of finding the time-dependent thermal conductivity $a(t)$, the space-dependent component of the fluid velocity $b(x)$ or, of the absorbtion (perfusion) coefficient $c(x)$, together with the temperature $u(x, t)$, which satisfy the parabolic heat equation

$$\frac{\partial u}{\partial t}(x,t) = a(t)\left(\frac{\partial^2 u}{\partial x^2}(x,t) + b(x)\frac{\partial u}{\partial x}(x,t) - c(x)u(x,t)\right) + f(x,t), \quad (x,t) \in Q_T, \quad (1)$$

the initial condition

$$u(x,0) = \phi(x), \qquad 0 \le x \le L, \quad (2)$$

the Dirichlet boundary conditions

$$u(0,t) = \mu_1(t), \qquad u(L,t) = \mu_2(t), \qquad 0 \le t \le T, \quad (3)$$

the heat flux Neumann condition

$$-a(t)u_x(0,t) = \mu_3(t), \qquad 0 \le t \le T. \quad (4)$$

and the time-average condition

$$\int_0^{T_0} a(t)u(x,t)dt = \psi(x), \qquad 0 \le x \le L, \quad (5)$$

where $T_0 \in (0, T]$ is a given fixed number. We note that the single identifications of the coefficient $b(x)$ or $c(x)$, when $a(t)$ is known and taken to be unity, have been investigated elsewhere in [14, 15].

Equation (5) is a new overdetermination condition that in the case of heat conduction, can be regarded as the total potential heat function whose derivative, if it exists,

$$\int_0^{T_0} a(t)u_x(x,t)dt = \psi'(x), \quad 0 \le x \le L, \quad (6)$$

yields the time-average of the heat flux over the time period $[0, T_0]$. We consider therefore the following two inverse problems concerning the simultaneous determination of the coefficients $a(t)$ and $b(x)$ when $c = 0$, termed the Inverse Problem I, and of the coefficients $a(t)$ and $c(x)$ when $b = 0$, termed the Inverse Problem II. These inverse problems have been previously investigated theoretically by Ivanchov [12, Chapter 5], who establish their existence and uniqueness, as follows.

2.1 Inverse problem I

In this case $c = 0$ and equation (1) becomes

$$\frac{\partial u}{\partial t}(x,t) = a(t)\left(\frac{\partial^2 u}{\partial x^2}(x,t) + b(x)\frac{\partial u}{\partial x}(x,t)\right) + f(x,t), \quad (x,t) \in Q_T. \tag{7}$$

Then the inverse problem I requires determining the triplet solution $(a(t), b(x), u(x,t)) \in C[0,T] \times H^{\gamma}[0,L] \times H^{2+\gamma,1}(\overline{Q}_T)$ for some $\gamma \in (0,1)$, $a(t) > 0$ for $t \in [0,T]$, that satisfies equations (2)–(4), (6) and (7). For the definition of the spaces involved, see [16]. In particular, $H^{\gamma}[0,L]$ denotes the space of Hölder continuous functions with exponent γ and $H^{2+\gamma,1}(\overline{Q}_T)$ denotes the space of continuous functions u along with their partial derivatives u_x, u_{xx}, u_t in $\overline{Q}_T$ and with u_{xx} being Hölder continuous with exponent γ in $x \in [0,L]$ uniformly with respect to $t \in [0,T]$.

Theorem 1 (Existence, see Theorem 5.2.1 of [12]). *Suppose that the following conditions hold:*

1. $\phi \in H^{2+\gamma}[0,L]$, $\psi \in H^{2+\gamma}[0,L]$, $\mu_i \in C^1[0,T]$ *for* $i = 1,2$, $\mu_3 \in C[0,T]$, $f \in H^{\gamma,0}(\overline{Q}_T)$;
2. $\phi'(x) > 0$, $\psi'(x) > 0$ *for* $x \in [0,L]$, $\mu_3(t) < 0$ *for* $t \in [0,T]$;
3. $\phi(0) = \mu_1(0)$, $\phi(L) = \mu_2(0)$, $\psi'(0) = -\int_0^{T_0} \mu_3(t)dt$, $\mu_1'(0) = a(0)(\phi''(0)+b(0)\phi'(0))+ f(0,0)$, $\mu_2'(0) = a(0)(\phi''(L) + b(L)\phi'(L)) + f(L,0)$, *where* $a(0)$, $b(0)$ *and* $b(L)$ *are determined by* $a(0) = -\mu_3(0)/\phi'(0)$,

$$b(0) = \frac{1}{\psi'(0)}\left(\mu_1(T_0) - \phi(0) - \psi''(0) - \int_0^{T_0} f(0,t)dt\right),$$
$$b(L) = \frac{1}{\psi'(L)}\Big(\mu_2(T_0) - \phi(L) - \psi''(L) - \int_0^{T_0} f(L,t)dt\Big).$$

Then, if T_0 *is sufficiently small, the inverse problem (2)–(4), (6) and (7) has a solution determined for* $(x,t) \in \overline{Q}_{T_0} := [0,L] \times [0,T_0]$.

In the above, $H^{2+\gamma}[0,L]$ denotes the space of twice continuously differentiable functions with the second-order derivative being Hölder continuous with exponent γ in $[0,L]$. Note that according to Theorem 1 of [11], the existence result in the above theorem also holds if $f \in C^{1,0}(\overline{Q}_T)$ and if condition 2 is replaced by:

2′. $\phi(x) \le 0$, $\phi'(x) \ge 0$, $\psi'(x) > 0$ *for* $x \in [0,L]$, $\phi'(0) > 0$, $\mu_3(t) < 0$, $\mu_1(t) \le 0$, $\mu_2(t) \le 0$, $\mu_1'(t) \le f(0,t)$, $\mu_2'(t) \ge f(L,t)$ *for* $t \in [0,T]$, $f(x,t) \le 0$, $f_x(x,t) \ge 0$ *for* $(x,t) \in \overline{Q}_T$.

Theorem 2 (Uniqueness, see Theorem 5.2.2 of [12]). *If the conditions*

$$\mu_3(t) \neq 0 \quad \text{for } t \in [0,T], \quad \psi'(x) \neq 0 \quad \text{for } x \in [0,L]$$

hold, then, if T_0 is sufficiently small, the solution of the inverse problem (2)–(4), (6) and (7) is unique for $(x,t) \in \overline{Q}_{T_0}$.

2.2 Inverse problem II

In this case $b = 0$ and equation (1) becomes

$$\frac{\partial u}{\partial t}(x,t) = a(t)\left(\frac{\partial^2 u}{\partial x^2}(x,t) - c(x)u(x,t)\right) + f(x,t), \quad (x,t) \in Q_T. \tag{8}$$

Then the inverse problem II requires determining the triplet solution $(a(t), c(x), u(x,t)) \in C[0,T] \times H^{\gamma}[0,L] \times H^{2+\gamma,1}(\overline{Q}_T)$, $a(t) > 0$ for $t \in [0,T]$, $c(x) \geq 0$ for $x \in [0,L]$, that satisfies equations (2)–(5) and (8).

Theorem 3 (Existence, see [10], and Theorem 5.1.1 of [12]). *Suppose that the following conditions hold:*

1. $\phi \in H^{2+\gamma}[0,L]$, $\psi \in H^{2+\gamma}[0,L]$, $\mu_i \in C^1[0,T]$ *for* $i = 1,2$, $\mu_3 \in C[0,T]$, $f \in C^{2,0}(\overline{Q}_T)$;

2. $\phi(x) \geq 0$, $\phi'(x) > 0$, $\phi''(x) \leq 0$, $\psi(x) > 0$, $\psi''(x) \geq 0$ *for* $x \in [0,L]$, $\mu_i(t) \geq 0$ *for* $i = 1,2$, $\mu_3(t) < 0$, $\mu_1(t) - \phi(0) - \int_0^t f(0,\tau)d\tau \leq 0$, $\mu_2(t) - \phi(L) - \int_0^t f(L,\tau)d\tau \leq 0$ *for* $t \in [0,T]$, $f(x,t) \geq 0$, $f_{xx}(x,t) \leq 0$ *for* $(x,t) \in \overline{Q}_T$;

3. $\phi(0) = \mu_1(0)$, $\phi(L) = \mu_2(0)$, $\psi'(0) = -\int_0^{T_0} \mu_3(t)dt$, $\mu_1'(0) = a(0)(\phi''(0) - c(0)\phi(0)) + f(0,0)$, $\mu_2'(0) = a(0)(\phi''(L) - c(L)\phi(L)) + f(L,0)$, *where* $a(0)$, $c(0)$ *and* $c(L)$ *are determined by* $a(0) = -\mu_3(0)/\phi'(0)$,

$$c(0) = -\frac{1}{\psi(0)}\left(\mu_1(T_0) - \phi(0) - \psi''(0) - \int_0^{T_0} f(0,t)dt\right),$$
$$c(L) = -\frac{1}{\psi(L)}\Big(\mu_2(T_0) - \phi(L) - \psi''(L) - \int_0^{T_0} f(L,t)dt\Big).$$

Then, if T_0 is sufficiently small, the inverse problem (2)–(5) and (8) has a solution determined for $(x,t) \in \overline{Q}_{T_0}$.

Theorem 4 (Uniqueness, see Theorem 5.1.2 of [12]). *If the conditions*

$$\mu_3(t) \neq 0 \quad \text{for } \ t \in [0,T], \quad \psi(x) \neq 0 \quad \text{for } \ x \in [0,L]$$

hold, then, if T_0 is sufficiently small, the solution of the inverse problem (2)–(5) and (8) is unique for $(x,t) \in \overline{Q}_{T_0}$.

3 Solution of direct problem

In this section, we consider the direct (forward) initial boundary value problem given by equations (1)–(3) in which the coefficients $a(t)$, $b(x)$ and $c(x)$ are known and $f(x,t)$, $\phi(x)$ and $\mu_i(t)$, for $i = 1, 2$, are given, and the temperature $u(x,t)$ is the solution to be determined.

The discrete form of this direct problem is as follows. Take two positive integers M and N and let $\Delta x = L/M$ and $\Delta t = T/N$ be the uniform step lengths in space and time direction, respectively. We subdivide the solution domain $Q_T = (0, L) \times (0, T)$ into $M \times N$ subintervals of equal length. At the node (i, j) we denote $u_{i,j} = u(x_i, t_j)$, $a_j = a(t_j)$, $b_i = b(x_i)$, $c_i = c(x_i)$ and $f_{i,j} = f(x_i, t_j)$, where $x_i = i\Delta x$, $t_j = j\Delta t$ for $i = \overline{0, M}$, $j = \overline{0, N}$.

Considering the general form of partial differential equation (1) as

$$u_t = G(x, t, u, u_x, u_{xx}), \tag{9}$$

the Crank-Nicolson finite-difference method, [8, 23], discretises (9), (2) and (3) as

$$\frac{u_{i,j+1} - u_{i,j}}{\Delta t} = \frac{1}{2}\left(G_{i,j} + G_{i,j+1}\right), \qquad i = \overline{1, (M-1)},\ j = \overline{0, (N-1)}, \tag{10}$$

$$u_{i,0} = \phi(x_i), \qquad i = \overline{0, M}, \tag{11}$$

$$u_{0,j} = \mu_1(t_j), \qquad u_{M,j} = \mu_2(t_j), \qquad j = \overline{0, N}, \tag{12}$$

where

$$G_{i,j} = G\left(x_i, t_j, u_{i,j}, \frac{u_{i+1,j} - u_{i-1,j}}{2(\Delta x)}, \frac{u_{i+1,j} - 2u_{i,j} + u_{i-1,j}}{(\Delta x)^2}\right), \qquad i = \overline{1, (M-1)},\ j = \overline{0, (N-1)}. \tag{13}$$

For our model, equation (1) can be discretised in the form of (10) as

$$-A_{i,j+1}u_{i-1,j+1} + (1 + B_{i,j+1})u_{i,j+1} - C_{i,j+1}u_{i+1,j+1} = A_{i,j}u_{i-1,j} + (1 - B_{i,j})u_{i,j} + C_{i,j}u_{i+1,j} + \frac{\Delta t}{2}\left(f_{i,j} + f_{i,j+1}\right) \tag{14}$$

for $i = \overline{1, (M-1)}$, $j = \overline{0, N}$, where

$$A_{i,j} = \frac{(\Delta t)a_j}{2(\Delta x)^2} - \frac{a_j b_i (\Delta t)}{4(\Delta x)}, \quad B_{i,j} = \frac{(\Delta t)a_j}{(\Delta x)^2} + \frac{(\Delta t)a_j c_i}{2}, \quad C_{i,j} = \frac{(\Delta t)a_j}{2(\Delta x)^2} + \frac{a_j b_i (\Delta t)}{4(\Delta x)}.$$

At each time step t_{j+1} for $j = \overline{0, (N-1)}$, using the Dirichlet boundary conditions (12), the above difference equation can be reformulated as a $(M-1) \times (M-1)$ system of linear equations of the form,

$$D\mathbf{u}_{j+1} = \mathrm{E}\mathbf{u}_j + \mathbf{b}, \tag{15}$$

where

$$\mathbf{u}_{j+1} = (u_{1,j+1}, u_{2,j+1}, ..., u_{M-1,j+1})^{\mathrm{T}},$$

$$D = \begin{pmatrix} 1-B_{1,j+1} & -C_{1,j+1} & 0 & \cdots & 0 & 0 & 0 \\ -A_{2,j+1} & 1-B_{2,j+1} & -C_{2,j+1} & \cdots & 0 & 0 & 0 \\ \vdots & \vdots & \vdots & \ddots & \vdots & \vdots & \vdots \\ 0 & 0 & 0 & \cdots & -A_{M-2,j+1} & 1-B_{M-2,j+1} & -C_{M-2,j+1} \\ 0 & 0 & 0 & \cdots & 0 & -A_{M-1,j+1} & 1-B_{M-1,j+1} \end{pmatrix},$$

$$E = \begin{pmatrix} 1-B_{1,j} & C_{1,j} & 0 & \cdots & 0 & 0 & 0 \\ A_{2,j} & 1-B_{2,j} & C_{2,j} & \cdots & 0 & 0 & 0 \\ \vdots & \vdots & \vdots & \ddots & \vdots & \vdots & \vdots \\ 0 & 0 & 0 & \cdots & A_{M-2,j} & 1-B_{M-2,j} & C_{M-2,j} \\ 0 & 0 & 0 & \cdots & 0 & A_{M-1,j} & 1-B_{M-1,j} \end{pmatrix},$$

and

$$\mathbf{b} = \begin{pmatrix} \frac{\Delta t}{2}(f_{1,j}+f_{1,j+1}) + A_{1,j+1}\mu_1(t_{j+1}) \\ \frac{\Delta t}{2}(f_{2,j}+f_{2,j+1}) \\ \vdots \\ \frac{\Delta t}{2}(f_{M-2,j}+f_{M-2,j+1}) \\ \frac{\Delta t}{2}(f_{M-1,j}+f_{M-1,j+1}) + C_{M-1,j+1}\mu_2(t_{j+1}) \end{pmatrix}.$$

3.1 Example

As an example, consider the direct problem (1)–(3) and with $T = L = 1$ and

$$\begin{aligned} a(t) = e^t, \quad b(x) = 2-x, \quad c(x) = \frac{1}{1+x}, \quad \phi(x) = u(x,0) = x^2 + x, \\ \mu_1(t) = u(0,t) = 2t, \quad \mu_2(t) = u(1,t) = 2+2t, \\ f(x,t) = 2 - 2e^t\left(2 + x - x^2 - \frac{t}{1+x}\right). \end{aligned}$$

The exact solution is given by

$$u(x,t) = x^2 + x + 2t, \quad (x,t) \in \overline{Q}_T. \tag{16}$$

Outputs of interest are the heat flux (4) and the total potential heat function (5) on the time period $[0, T_0]$, say $T_0 = 1$,

$$\mu_3(t) = -a(t)u_x(0,t) = -e^t, \quad t \in [0,1], \tag{17}$$

$$\psi(x) = \int_0^1 a(t)u(x,t)dt = (x^2+x)(e-1) + 2, \quad x \in [0,1], \tag{18}$$

and its derivative (6) given by

$$\psi'(x) = \int_0^1 a(t)u_x(x,t)dt = (2x+1)(e-1), \quad x \in [0,1]. \tag{19}$$

The numerical and exact solutions for $u(x,t)$ at interior points are shown in Figure 1 and also the absolute error between them is included. One can notice that an excellent agreement is obtained. Figures 2(a)–(c) show the numerical solutions in comparison with

the exact ones (17)–(19) for $\mu_3(t)$, $\psi(x)$ and $\psi'(x)$, respectively. These have been calculated using the following $O((\Delta x)^2)$ finite-difference approximation formula and trapezoidal rule for integrals:

$$\mu_3(t_j) = -a(t_j)u_x(0,t_j) = -\frac{(4u_{1,j} - u_{2,j} - 3u_{0,j})a_j}{2(\Delta x)}, \quad j = \overline{0,N}, \tag{20}$$

$$\psi(x_i) = \int_0^1 a(t)u(x_i,t)dt = \frac{1}{2N}\left(a_0u_{i,0} + a_Nu_{i,N} + 2\sum_{j=1}^{N-1} u_{i,j}\right), \quad i = \overline{0,M}, \tag{21}$$

$$\begin{aligned}\psi'(x_i) &= \int_0^1 a(t)u_x(x_i,t)dt \\ &= \frac{1}{2N}\begin{cases} a_0\phi'(0) + a_Nu_x(0,t_N) + 2\sum_{j=1}^{N-1} a_ju_x(0,t_j), & \text{if } i = 0; \\ a_0\phi'(x_i) + a_Nu_x(x_i,t_N) + 2\sum_{j=1}^{N-1} a_ju_x(x_i,t_j), & \text{if } i = \overline{1,M-1}; \\ a_0\phi'(1) + a_Nu_x(1,t_N) + 2\sum_{j=1}^{N-1} a_ju_x(1,j), & \text{if } i = M, \end{cases}\end{aligned} \tag{22}$$

where, for $j = \overline{0,N}$,

$$u_x(0,t_j) = \frac{4u_{1,j} - u_{2,j} - 3u_{0,j}}{2(\Delta x)}, \tag{23}$$

$$u_x(1,t_j) = -\frac{4u_{M-1,j} - u_{M-2,j} - 3u_{M,j}}{2(\Delta x)}, \tag{24}$$

$$u_x(x_i,t_j) = \frac{u_{i+1,j} - u_{i-1,j}}{2(\Delta x)} \quad i = \overline{1,(M-1)}. \tag{25}$$

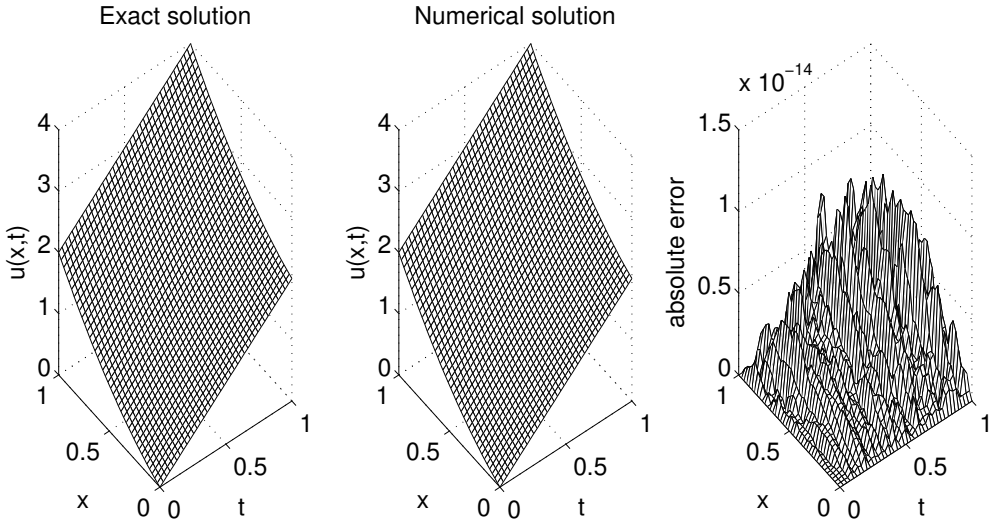

Figure 1: Exact and numerical solutions for the temperature $u(x,t)$, and the absolute error for the direct problem obtained with $M = N = 40$.

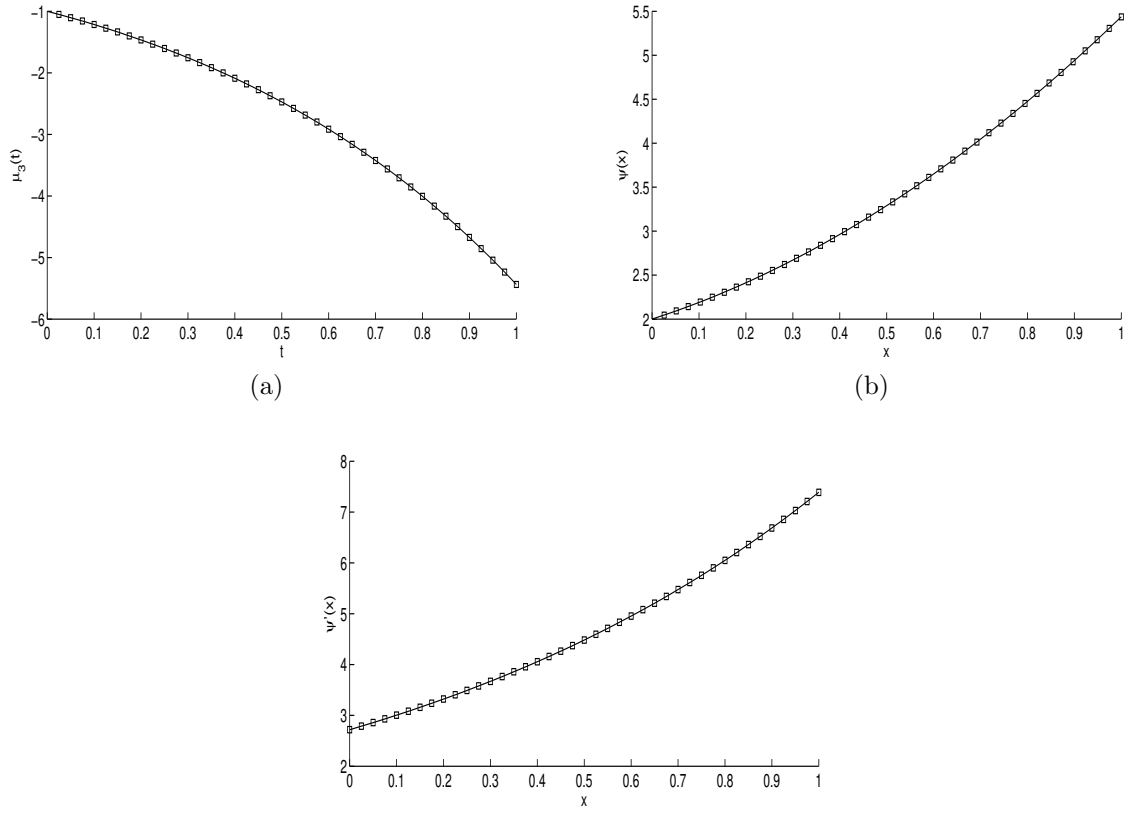

Figure 2: Exact (—) and numerical (□□□) solutions for: (a) the heat flux $\mu_3(t)$, (b) the total potential function $\psi(x)$, and (c) the time-average heat flux $\psi'(x)$, for the direct problem obtained with $M = N = 40$.

4 Numerical approach to the inverse problems

The inverse problems under investigation are nonlinear and the most common numerical approach is to impose the overdetermination conditions in a least-squares sense, based on minimizing the objective function

$$F_I(a,b) := \big\|a(t)u_x(0,t) + \mu_3(t)\big\|^2 + \Big\| \int_0^{T_0} a(t)u_x(x,t)dt - \psi'(x)\Big\|^2 + \beta_1\big\|a(t)\big\|^2 + \beta_2\big\|b(x)\big\|^2, \tag{26}$$

for the inverse problem I, and

$$F_{II}(a,c) := \big\|a(t)u_x(0,t) + \mu_3(t)\big\|^2 + \Big\| \int_0^{T_0} a(t)u(x,t)dt - \psi(x)\Big\|^2 + \beta_1\big\|a(t)\big\|^2 + \beta_3\big\|c(x)\big\|^2, \tag{27}$$

for the inverse problem II, where $\beta_i \geq 0$ for $i = 1, 2, 3$ are regularization parameters to be prescribed and the norms are understood in the L^2-sense.

Of course, finding a global minimizer to these nonlinear optimization problems is in general not an easy task. Since the inverse problems under investigation are nonlinear

the functionals (26) and (27) are not convex and could have many local minima in which, depending on the initial guess, a descent-based method tends to get stuck if the underlying problems are ill-posed, [3, p.17]. A possible way to deal with this difficulty could be to develop a "global convergent method", [1, 21], whose convergence to a good approximation of the exact solution is independent of the initial guess but this challenging task is deferred to a future work.

Bearing in mind that the values of $a(0)$, $b(0)$, $b(L)$, $c(0)$ and $c(L)$ are determined *a priori* directly form the compatibility conditions in Theorems 1 and 3, the discretizations of (26) and (27) simplify as

$$F_I(\underline{a},\underline{b}) = \sum_{j=1}^{N}\Big[a_j u_x(0,t_j)+\mu_3(t_j)\Big]^2 + \sum_{i=1}^{M-1}\Big[\int_0^{T_0} a(t)u_x(x_i,t)dt - \psi'(x_i)\Big]^2 + \beta_1\sum_{j=1}^{N} a_j^2 + \beta_2\sum_{i=1}^{M-1} b_i^2, \tag{28}$$

$$F_{II}(\underline{a},\underline{c}) = \sum_{j=1}^{N}\Big[a_j u_x(0,t_j)+\mu_3(t_j)\Big]^2 + \sum_{i=1}^{M-1}\Big[\int_0^{T_0} a(t)u(x_i,t)dt - \psi(x_i)\Big]^2 + \beta_1\sum_{j=1}^{N} a_j^2 + \beta_3\sum_{i=1}^{M-1} c_i^2. \tag{29}$$

In the case when $\beta_1 = \beta_2 = \beta_3 = 0$, the above functions become the ordinary least-squares functionals which normally produce unstable solutions for noisy measurements (4)–(6). The minimization of the functions (28) and (29) subject to the physical simple lower bounds for $a(t) > 0$ and $c(x) \geq 0$ is accomplished via the MATLAB optimization toolbox *lsqnonlin*, [18]. This routine aims to solve nonlinear least-squares (nonlinear data-fitting) problems and find the minimum of a scalar function of several variables starting from an initial guess subject to constraints. This initial guess, say $(a^0(t),\, b^0(x))$ for inverse problem I, could be included in (26) by replacing the last two terms in it by $\beta_1\|a(t)-a^0(t)\|^2+\beta_2\|b(x)-b^0(x)\|^2$, but this is not necessary, see [3, p.18]. Alternatively, one could use a truncated Gauss-Newton method with simple bounds on the variables, [13], for solving the constrained nonlinear optimization problem. We use the Trust-Region-Reflective (TRR) algorithm, and the positive components of the vector $\underline{a}$ and the non-negative components of the vector $\underline{c}$ are sought in the intervals $[10^{-10}, 10^3]$ and $[0, 10^3]$, respectively.

We also take the parameters of the routine as follows:

- Number of variables $M = N = 20$ for inverse problem I and $M = N = 40$ for inverse problem II.
- Maximum number of iterations = 20 × (number of variables).
- Maximum number of objective function evaluations = 10^3 × (number of variables).
- Solution tolerance (xTol) = 10^{-20}.
- Object function tolerance (FunTol) = 10^{-20}.

For an objective function $F(x)$, the tolerance FunTol is defined as $|F(x_i) - F(x_{i+1})| <$ FunTol$(1+|F(x_i)|)$ and the solution tolerance xTol is defined as $|x_i - x_{i+1}| <$ xTol$(1+|x_i|)$, see [18].

The inverse problems under investigation are solved subject to both exact and noisy data which are numerically simulated as

$$\mu_3^{\epsilon 1}(t_j) = \mu_3(t_j) + \epsilon 1_j, \quad j = \overline{1, N}, \tag{30}$$

$$\psi'^{\epsilon 2}(x_i) = \psi'(x_i) + \epsilon 2_i, \quad i = \overline{1, (M-1)}, \tag{31}$$

$$\psi^{\epsilon 3}(x_i) = \psi(x_i) + \epsilon 3_i, \quad i = \overline{1, (M-1)}, \tag{32}$$

where $\epsilon 1_j$, $\epsilon 2_i$ and $\epsilon 3_i$ are random variables generated from Gaussian normal distributions with mean zero and standard deviations $\sigma 1$, $\sigma 2$ and $\sigma 3$ given by

$$\sigma 1 = p \times \max_{t\in[0,T]} |\mu_3(t)|, \quad \sigma 2 = p \times \max_{x\in[0,L]} |\psi'(x)|, \quad \sigma 3 = p \times \max_{x\in[0,L]} |\psi(x)|, \tag{33}$$

where p represents the percentage of noise. We use the MATLAB function *normrnd* to generate the random variables $\underline{\epsilon 1} = (\epsilon 1_j)_{j=\overline{1,N}}$, $\underline{\epsilon 2} = (\epsilon 2_i)_{i=\overline{1,M-1}}$ and $\underline{\epsilon 3} = (\epsilon 2_i)_{i=\overline{1,M-1}}$, as follows:

$$\underline{\epsilon 1} = normrnd(0, \sigma 1, N),\ \underline{\epsilon 2} = normrnd(0, \sigma 2, M-1),\ \underline{\epsilon 3} = normrnd(0, \sigma 3, M-1). \tag{34}$$

5 Numerical results and discussion

In this section we present, discuss and assess the numerically obtained results by employing the FDM combined with Tikhonov regularization method, as presented in previous section, for a couple of benchmark test examples for each of the inverse problems I (Examples 1 and 2) and II (Examples 3 and 4). The root mean square errors ($rmse$)

$$rmse(a) = \sqrt{\frac{1}{N}\sum_{j=1}^{N} \left(a_{numerical}(t_j) - a_{exact}(t_j)\right)^2}, \tag{35}$$

$$rmse(b) = \sqrt{\frac{1}{M-1}\sum_{i=1}^{M-1} \left(b_{numerical}(x_i) - b_{exact}(x_i)\right)^2}, \tag{36}$$

$$rmse(c) = \sqrt{\frac{1}{M-1}\sum_{i=1}^{M-1} \left(c_{numerical}(x_i) - c_{exact}(x_i)\right)^2}, \tag{37}$$

were calculated in order to estimate the accuracy of the identified coefficients. In all examples we take $L = T_0 = T = 1$.

5.1 Example 1 (for inverse problem I)

In the first example, we consider the inverse problem I given by equations (2)–(4), (6) and (7) with the following input data:

$$\phi(x) = u(x,0) = x+1, \quad \mu_1(t) = u(0,t) = \frac{1}{1+t}, \quad \mu_2(t) = u(1,t) = \frac{2}{1+t},$$
$$\mu_3(t) = -a(t)u_x(0,t) = -1, \quad \psi'(x) = \int_0^1 a(t)u_x(x,t)dt = 1,$$
$$f(x,t) = -\frac{x+1}{(1+t)^2} + 2 - x.$$

One can observe that the conditions of Theorems 1 and 2 are satisfied, hence the problem is uniquely solvable. The analytical solution is given by

$$a(t) = 1+t, \quad b(x) = x-2, \quad u(x,t) = \frac{x+1}{1+t}. \tag{38}$$

The initial guess was $\underline{a}^0 = \underline{1}$ and $\underline{b}^0 = \underline{-2}$.

We consider first the case where there is no noise (i.e., $p = 0$) included in the input data $\mu_3(t)$ and $\psi'(x)$. In order to investigate the convergence of the numerical solutions for $a(t)$ and $b(x)$, the inverse problem was executed with various FDM mesh parameters, namely, $M = N \in \{10, 20, 40\}$ and the numerical results are compared with the exact ones in Table 1 and Figure 3. No regularization was included, i.e. $\beta_1 = \beta_2 = 0$ in (28). As illustrated in Figure 3 and more clearly in Table 1 one can be notice that, as $M = N$ increase, the numerical outputs converge to the exact values. The errors estimated through the $rmse(a)$ and $rmse(b)$ given by equations (35) and (36), respectively, are also included in Table 1. The decreasing behaviour of the errors with increasing the discretisation parameters clearly demonstrates the convergence and excellent accuracy of the numerically obtained solution. The number of iterations required to achieve the convergence of the objective functional (28) below a very low threshold of $O(10^{-20})$ also increases, as $M = N$ increase, as shown in Figure 4. From both Figures 3, 4 and Table 1, it can be seen that the independence of mesh is achieved with excellent accuracy and a rather coarse grid. Consequently, in what follows we fix $M = N = 20$ as a sufficiently fine mesh which ensures that a further refinement does not significantly affect the accuracy of the numerical results. Moreover, the rather low values for the number of variables result in a reasonable number of iterations and computational time to achieve the convergence of the objective function (28) which is minimized using the MATLAB toolbox routine *lsqnonlin*.

Table 1: The exact and the numerical coefficients $a(t)$ and $b(x)$, for Example 1 with no noise and no regularization, for $M = N \in \{10, 20, 40\}$. The $rmse(a)$ and $rmse(b)$ are also included.

t	0.1	0.2	...	0.9	1	M=N	$rmse(a)$
$a(t)$	1.1018	1.2016	...	1.8976	1.9971	10	1.7E-3
	1.1004	1.2004	...	1.8994	1.9993	20	4.0E-4
	1.1001	1.2001	...	1.8998	1.9998	40	9.8E-5
	1.1000	1.2000	...	1.9000	2.0000	exact	0
x	0.1	0.2	...	0.8	0.9	M=N	$rmse(b)$
$b(x)$	-1.8983	-1.7981	...	-1.1972	-1.0971	10	2.4E-3
	-1.8996	-1.7995	...	-1.1993	-1.0993	20	5.9E-4
	-1.8999	-1.7999	...	-1.1998	-1.0998	40	1.4E-4
	-1.9000	-1.8000	...	-1.2000	-1.1000	exact	0

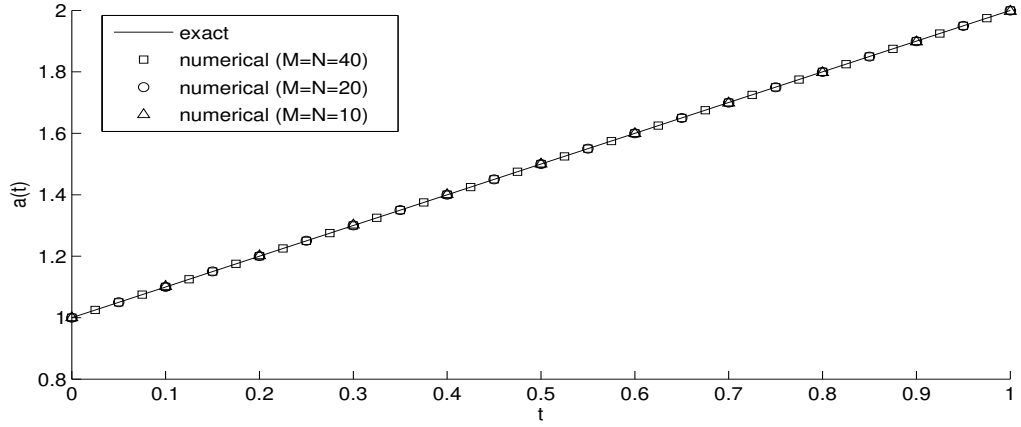

(a)

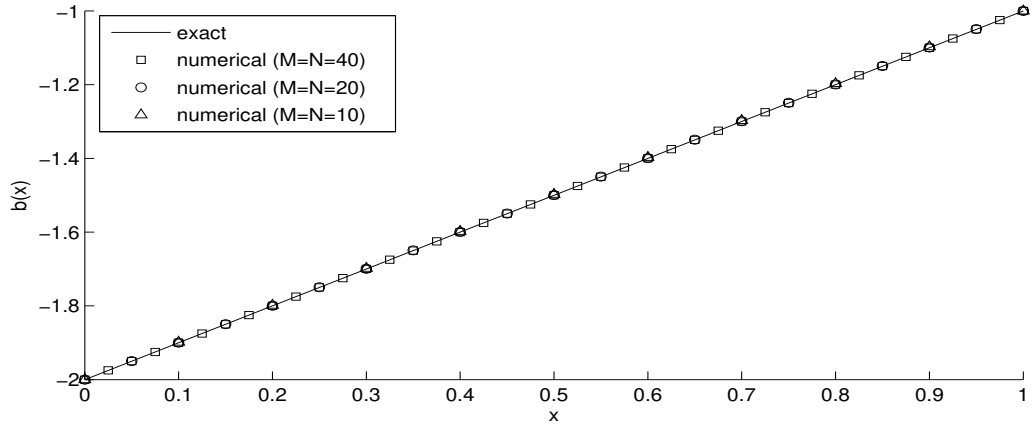

(b)

Figure 3: The coefficients (a) $a(t)$, and (b) $b(x)$ for Example 1 with no noise and no regularization, for $M = N \in \{10, 20, 40\}$.

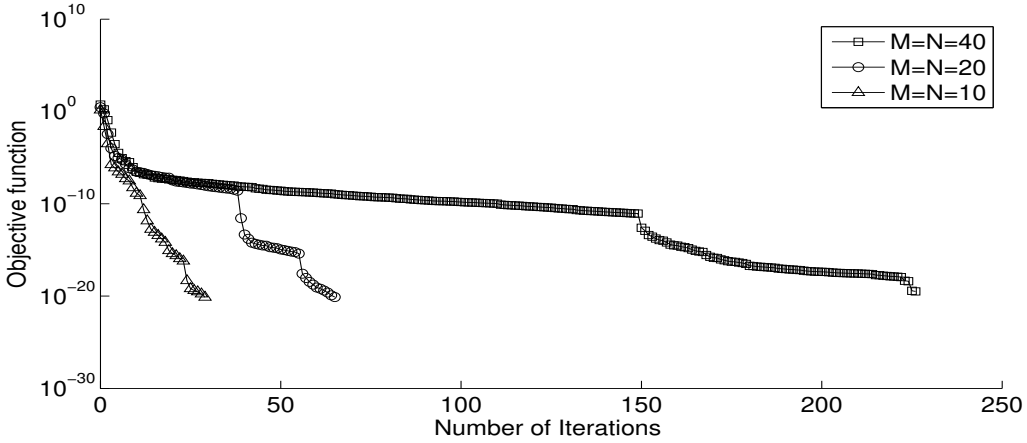

Figure 4: Objective function (28), for Example 1 with no noise and no regularization, for $M = N \in \{10, 20, 40\}$.

Even though the Theorems 1 and 2 ensure the unique solvability of the inverse problem I, the problem is still ill-posed since small errors in input measurement can cause highly oscillating unbounded solutions. To overcome this instability, regularization such as the Tikhonov regularization method can be applied. The main difficulty in regularization of nonlinear ill-posed problems is the selection of regularization parameters. Many methods have been suggested to select such parameters which can be fairly applied to linear problems, but the selection in the nonlinear case is less reliable. In this paper, we choose the regularization parameters β_1 and β_2 by trial and error. We start with small values for regularization parameters and gradually increase them until numerical oscillations in the unknown coefficients disappear.

We fix $M = N = 20$ and we add $p = 2\%$ noise to the heat flux measurement (4) and the integral average of heat flux (6), as in (30) and (31), respectively, to test the stability. Figure 5 shows the convergence of the objective function (28), as a function of the number of iterations, for $\beta_1 = 0$ and various $\beta_2 \in \{0, 10^{-3}, 10^{-2}, 10^{-1}\}$. The minimization process was stopped if the maximum number of iterations or, the permitted tolerance has been reached. The associated numerical results for $a(t)$ and $b(x)$ are presented in Figure 6. From this figure it can be seen that the unregularized, i.e. $\beta_1 = \beta_2 = 0$, numerical results are much more stable for $a(t)$ than for $b(x)$. Therefore, in what follows in order to simplify the investigation and discussion we can solely take $\beta_1 = 0$ and assess the stability of the solution with respect to the single regularization parameter β_2 only. Overall, from Figure 6 (see also the numerical features summarized in Table 4 for Example 1) it can be seen that accurate and stable solutions are reconstructed when we choose the regularization parameter β_2 between 10^{-3} and 10^{-2}.

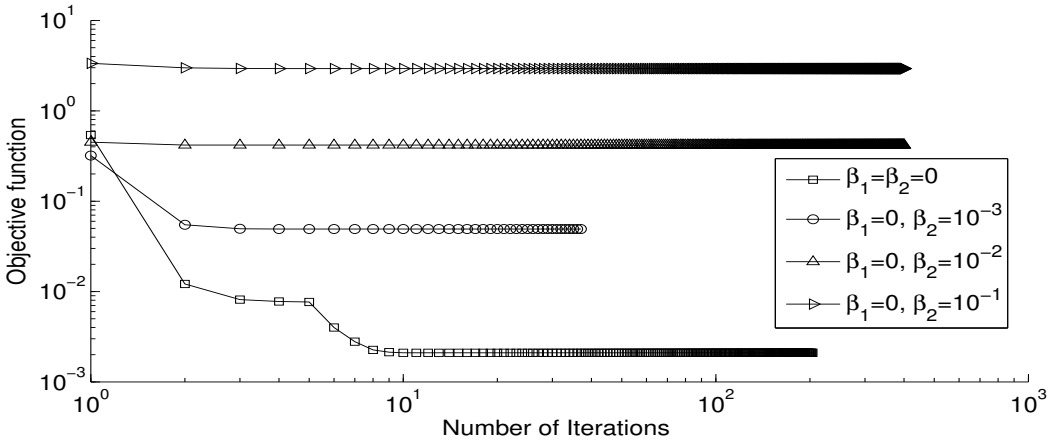

Figure 5: Objective function (28), for Example 1 with $p = 2\%$ noise and regularization.

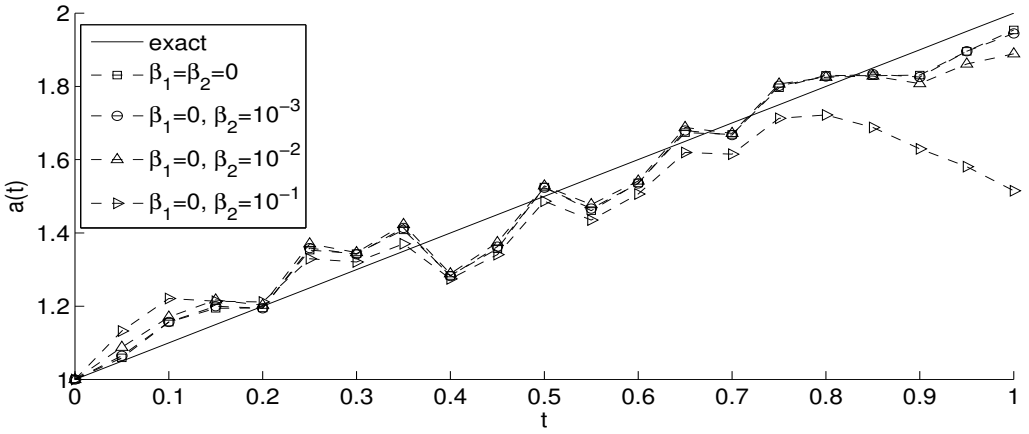

(a)

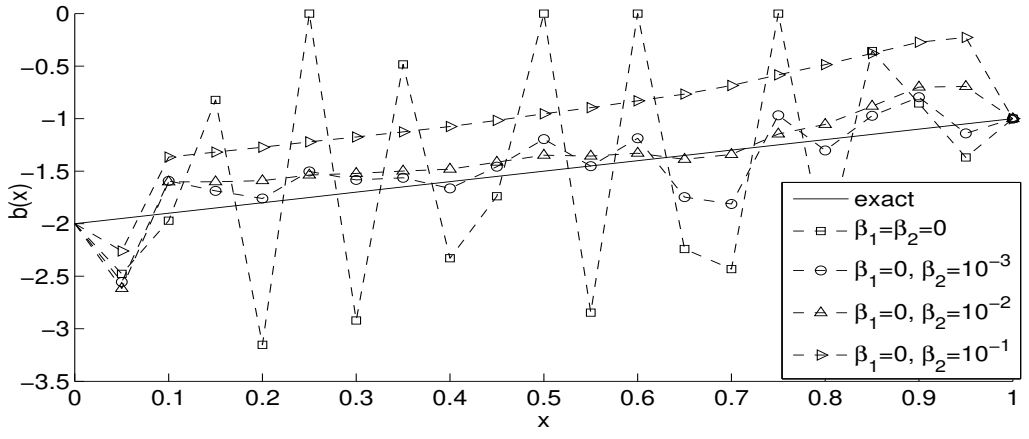

(b)

Figure 6: The coefficients (a) $a(t)$, and (b) $b(x)$ for Example 1 with $p = 2\%$ noise and regularization.

The reconstructions of the temperature $u(x, t)$ are presented in Figure 7. From this figure one can observe that, in general, the temperature is not affected significantly in terms of stability by the inclusion of noise.

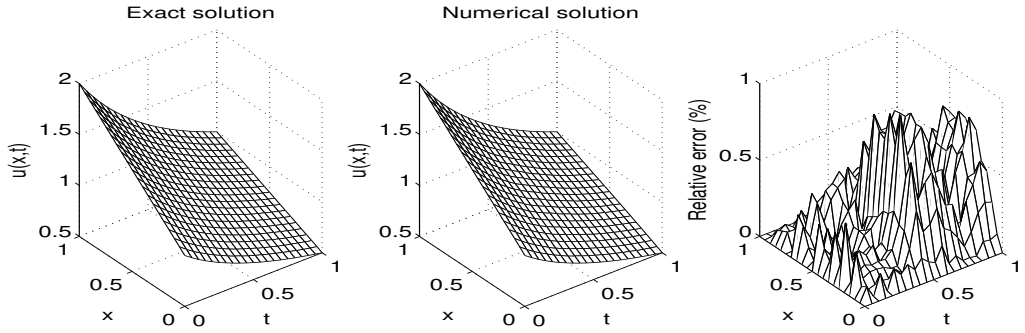

(a)

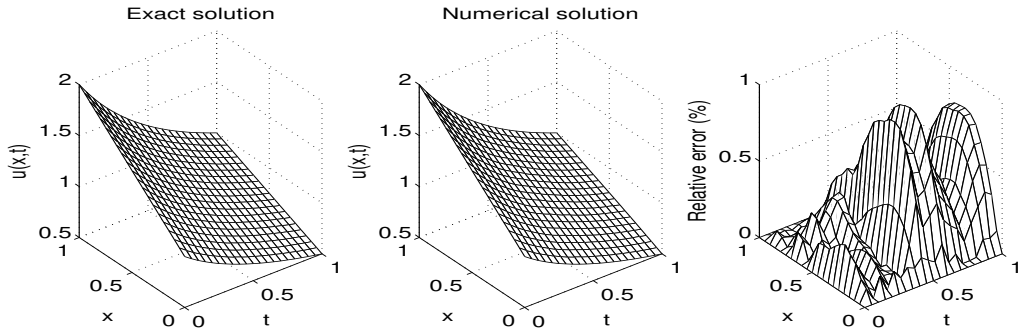

(b)

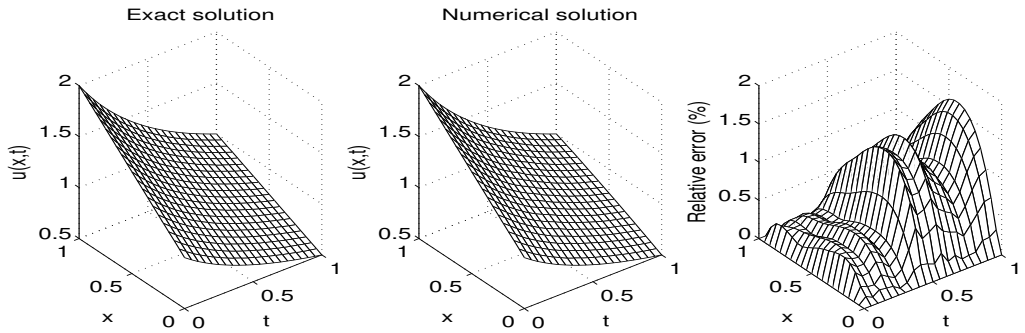

(c)

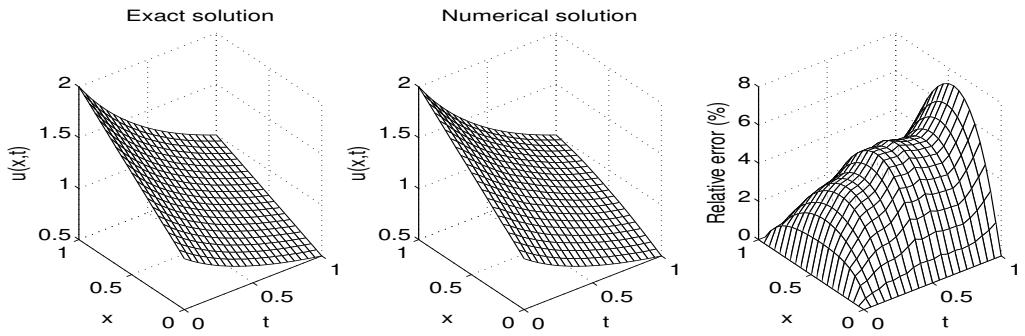

(d)

Figure 7: The exact and numerical temperatures $u(x,t)$, for Example 1, with $\beta_1 = 0$ and (a) $\beta_2 = 0$, (b) $\beta_2 = 10^{-3}$, (c) $\beta_2 = 10^{-2}$, and (d) $\beta_2 = 10^{-1}$, with $p = 2\%$ noise. The relative error between them is also included.

Next, in Table 2 we estimate the *rmse* errors (35) and (36) for various amounts of noise

$p \in \{1,2,3\}\%$ and various regularization parameters $\beta_2 \in \{0, 10^{-3}, 10^{-2}, 10^{-1}\}$. From this table it can be seen that stable solutions are achieved if regularization is included. Furthermore, the results become more accurate as the amount of noise decreases.

Table 2: The $rmse$ errors (35) and (36) for various amounts of noise $p \in \{1,2,3\}\%$ and various regularization parameters $\beta_1 = 0$ and $\beta_2 \in \{0, 10^{-3}, 10^{-2}, 10^{-1}\}$ for Example 1 .

	$rmse(a)$			$rmse(b)$		
$\beta_1 = 0$	$p = 1\%$	$p = 2\%$	$p = 3\%$	$p = 1\%$	$p = 2\%$	$p = 3\%$
$\beta_2 = 0$	0.0291	0.0595	0.0890	0.9507	1.0602	1.2718
$\beta_2 = 10^{-3}$	0.0322	0.0607	0.0907	0.1896	0.2668	0.3861
$\beta_2 = 10^{-2}$	0.0470	0.0691	0.0990	0.3105	0.2501	0.3539
$\beta_2 = 10^{-1}$	0.1775	0.1671	0.2082	0.6680	0.6043	0.6731

5.2 Example 2 (for inverse problem I)

In the previous example we have inverted linear and smooth coefficients given by equation (38). In this example, we consider the recovery of a smooth and nonlinear function for $a(t)$ and a non-smooth and piecewise linear function for $b(x)$ for the inverse problem I given by equations (2)–(4), (6) and (7) with the following input data:

$$\begin{aligned}
&\phi(x) = u(x,0) = x^3 + x, \quad \mu_1(t) = u(0,t) = t^2, \quad \mu_2(t) = u(1,t) = 2 + t + t^2,\\
&\mu_3(t) = -a(t)u_x(0,t) = -(1+t)(1+\cos^2(2\pi t)),\\
&\psi'(x) = \int_0^1 a(t)u_x(x,t)dt = \frac{9}{4}(1+2x^2),\\
&f(x,t) = x + 2t - 6x(1+\cos^2(2\pi t)) - (1+\cos^2(2\pi t))\left(\left|x - \frac{1}{2}\right| - 2\right)(3x^2 + t + 1).
\end{aligned}$$

One can observe that the conditions of Theorem 2 are satisfied, hence the solution is unique. The analytical solution is given by

$$a(t) = 1 + \cos^2(2\pi t), \quad b(x) = \left|x - \frac{1}{2}\right| - 2, \quad u(x,t) = x^3 + x + xt + t^2. \tag{39}$$

The initial guess was $\underline{a}^0 = \underline{2}$ and $\underline{b}^0 = \underline{-1.5}$.

We consider first the case of exact data, i.e. $p = 0$. We solve this nonlinear problem by minimizing the functional (28) which minimize the gap between the measured and the modeled data in equations (4) and (6). The numerical results for the unknown coefficients $a(t)$, $b(x)$ and the objective function plotted against the number of iterations are displayed in Figures 8 and 9. From these figures it can be seen that the numerical solutions for the coefficients $a(t)$ and $b(x)$ are convergent and accurate, as the FDM mesh is increased.

It is convenient to choose $M = N = 20$ for the rest of computations due to the reasonable accuracy and acceptable number of iterations cost to achieve convergence, see Table 3. From this table it can also be seen that the estimated errors $rmse(a)$ and $rmse(b)$ decrease monotonically to zero, as the FDM mesh size decreases to zero. For comparison purposes, we have also employed the MATLAB toolbox routine $fmincon$ based on the interior point algorithm, [18], instead of the TRR algorithm on which the $lsqnonlin$ routine is based, and the numerically obtained results are also included in Table

3 in brackets. By comparing in Table 3 the numerical results obtained using the two MATLAB toolbox routines *lsqnonlin* and *fmincon* for minimizing the objective function (28) one can observe that the $rmse(a)$ and $rmse(b)$ values are identical at least up to 4 decimals after comma which is reassuring to conclude that possibly an optimal accuracy has been achieved. The minimum values of (28) in both cases are very small indicating that the global minimum has been obtained. Finally, as expected, because *fmincon* is more general than *lsqnonlin* it performs more function evaluations and iterations to achieve convergence.

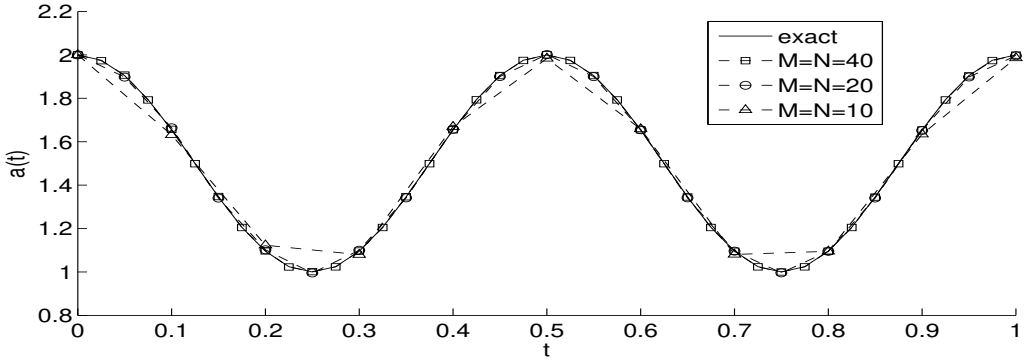

(a)

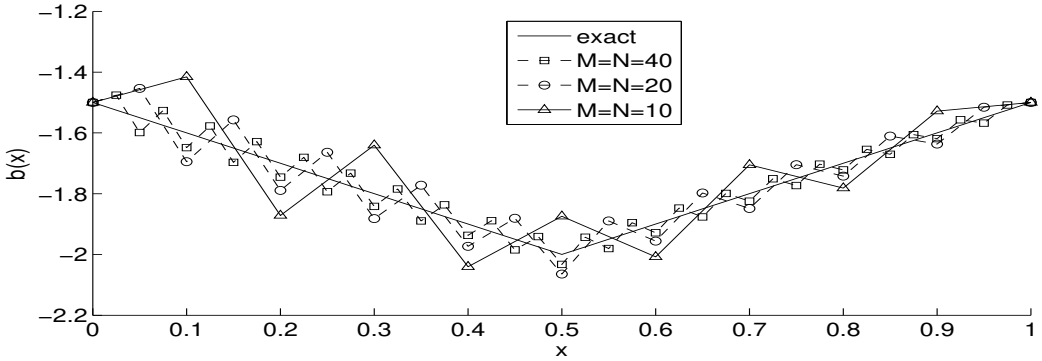

(b)

Figure 8: The coefficients (a) $a(t)$, and (b) $b(x)$ for Example 2 with no noise and no regularization, for $M = N \in \{10, 20, 40\}$.

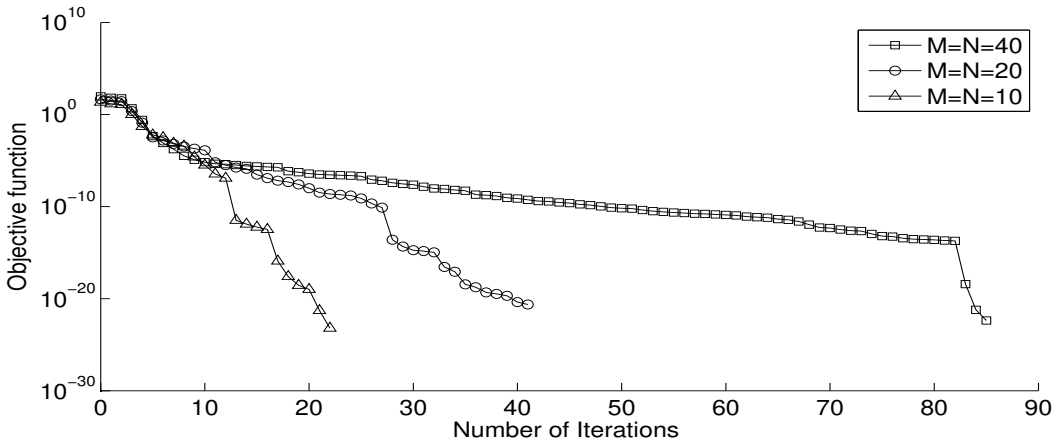

Figure 9: Objective function (28), for Example 2 with no noise no regularization, for $M = N \in \{10, 20, 40\}$.

Table 3: Number of iterations, number of function evaluations, value of objective function (28) at final iteration and the $rmse$ values (35) and (36), for Example 2 with no noise and no regularization, for $M = N \in \{10, 20, 40\}$, obtained using $lsqnonlin$ and $fmincon$ (in brackets).

$M = N$	10	20	40
No. of iterations	22 (85)	41 (167)	85 (446)
No. of function evaluations	529 (1986)	1806 (7254)	7138 (37142)
Minimum value of (28)	6.1E-24 (3.1E-15)	2.3E-21 (6E-15)	4.2E-23 (1.4E-14)
$rmse(a)$	0.0169 (0.0169)	0.0047 (0.0047)	0.0012 (0.0012)
$rmse(b)$	0.1321 (0.1321)	0.0685 (0.0685)	0.0349 (0.0349)

Next, the case of noise contamination with $p = 2\%$ is considered by adding Gaussian random noise into input data $\mu_3(t)$ and $\psi'(x)$ in (4) and (6), as in (30) and (31), respectively. As expected, without regularization, i.e., $\beta_1 = \beta_2 = 0$, the classical least-squares minimization produces an unstable solution. Hence, we employ the Tikhonov regularization method by adding stabilizing terms in (28) in order to restore the stability.

Figure 10 shows the objective function (28), as a function of the number of iterations. Form this figure it can be seen that convergence is achieved for each choice of regularization parameters. In case $\beta_1 = 0$ and $\beta_2 = 10^{-1}$, the minimization routine $lsqnonlin$ was stopped when the maximum number of iterations (Maxiter=400) was reached. In the other cases the iterative process was stopped when the objective function tolerance, or the solution tolerance has been reached.

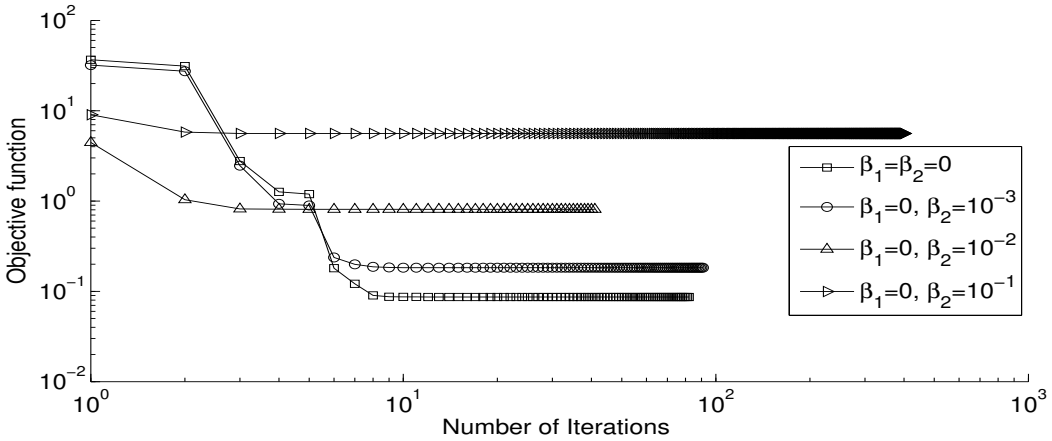

Figure 10: Objective function (28), for Example 2 with $p = 2\%$ noise and regularization.

Figure 11 displays the associated numerical results for the coefficients $a(t)$ and $b(x)$. From this figure and Table 4 it can be seen that accurate and stable results are obtained for $\beta_1 = 0$ and β_2 between 10^{-2} and 10^{-1}. As in Figure 6(a), one can notice once again that $\beta_1 = 0$ can be chosen because the retrieval of the thermal conductivity $a(t)$ is rather stable and is less influenced by noise, see Figures 8(a) and 11(a). Perhaps, this stability is due to the fact that this coefficient appears explicitly in the objective function (28), whilst $b(x)$ appears only implicitly.

Table 4: Number of iterations, number of function evaluations, value of regularized objective function (28) at final iteration, for Examples 1 and 2 with $\beta_1 = 0$ and $p = 2\%$ noise.

		$\beta_2 = 0$	$\beta_2 = 10^{-3}$	$\beta_2 = 10^{-2}$	$\beta_2 = 10^{-1}$
Example 1	No. of iterations	204	37	401	401
	No. of function evaluations	8815	1634	17286	17286
	Minimum value of (28)	0.0020	0.0491	0.4178	2.9329
	$rmse(a)$	0.0602	0.0607	0.0691	0.1671
	$rmse(b)$	1.0602	0.2668	0.2501	0.6043
Example 2	No. of iterations	82	91	41	401
	No. of function evaluations	3569	3956	1806	17286
	Minimum value of (28)	0.0865	0.1827	0.8105	5.5954
	$rmse(a)$	0.0501	0.0511	0.0483	0.0573
	$rmse(b)$	1.4860	1.3327	0.5415	0.3854

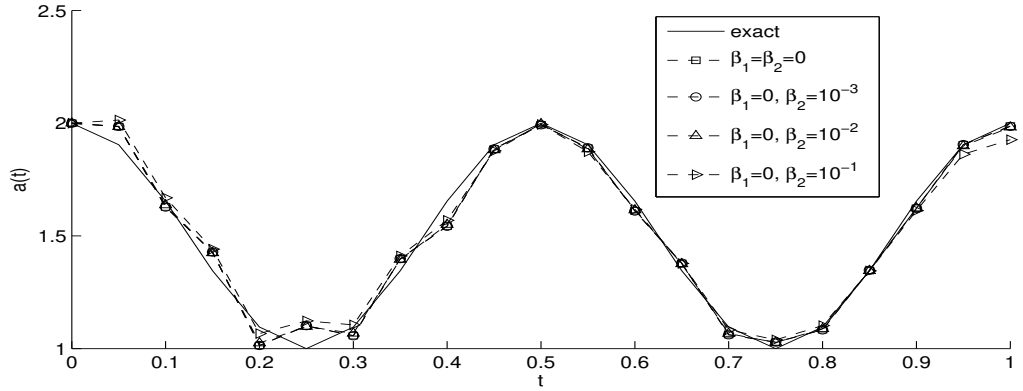

(a)

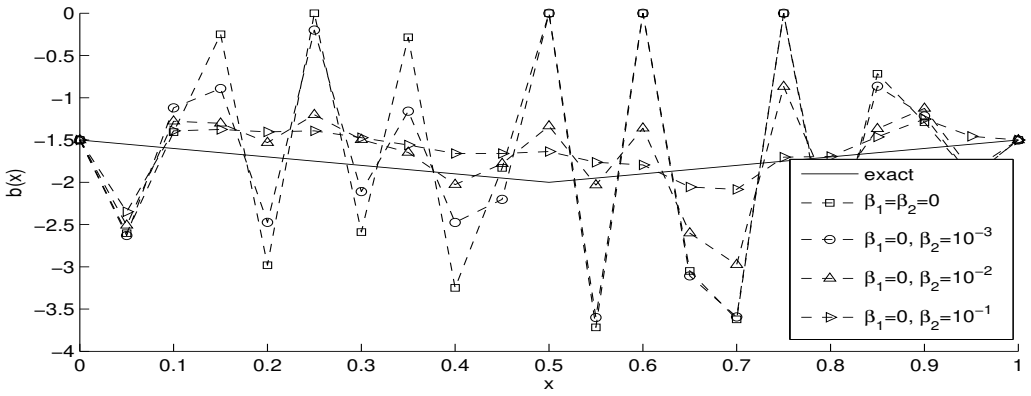

(b)

Figure 11: The coefficients (a) $a(t)$, and (b) $b(x)$ for Example 2 with $p = 2\%$ noise and regularization.

The exact and numerical temperatures are presented in Figure 12. As it also happened previously in Example 1 and illustrated in Figure 7, from Figure 12 it can be seen that the temperature reconstruction is not significantly affected by noise.

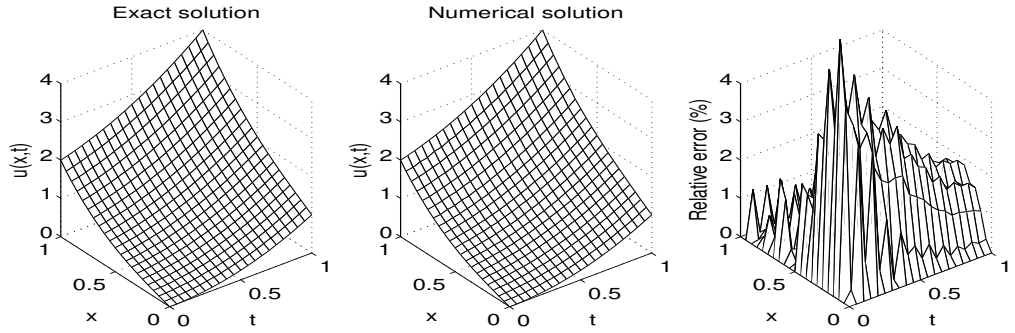

(a)

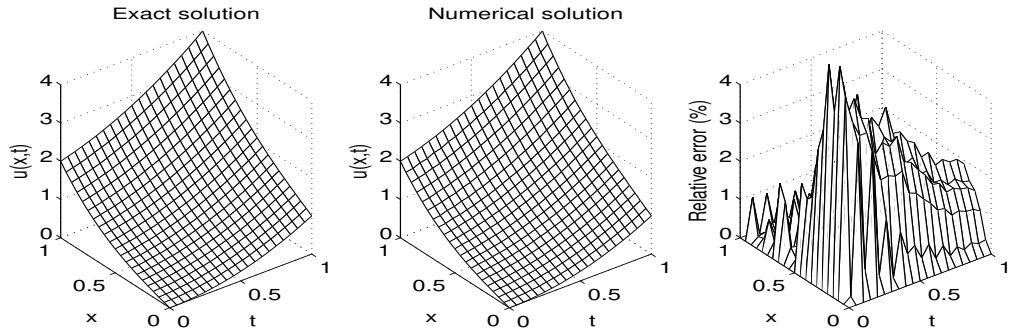

(b)

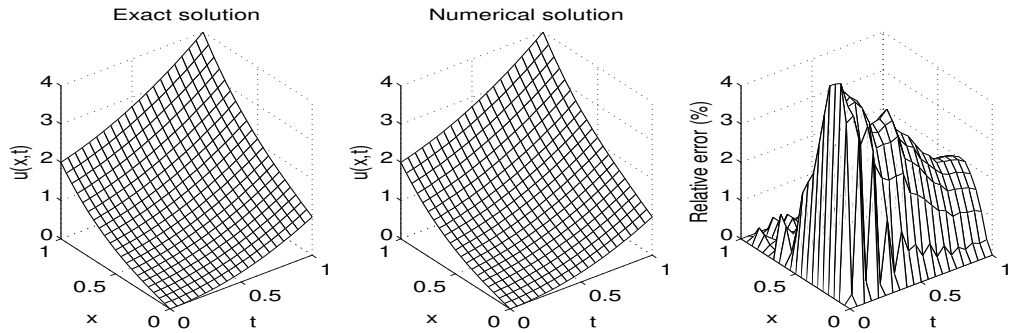

(c)

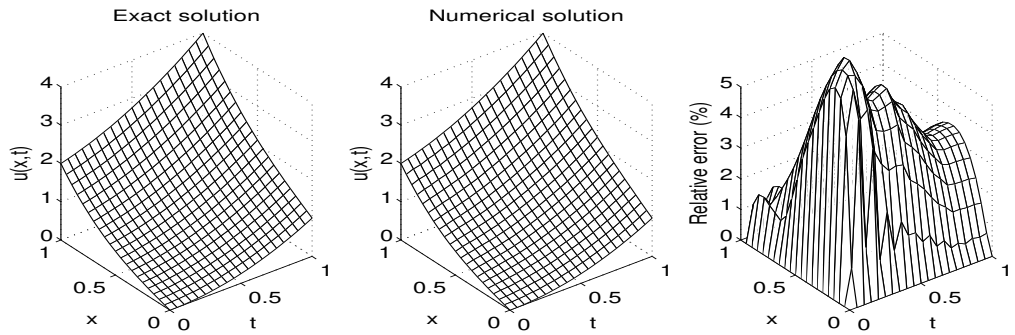

(d)

Figure 12: The exact and numerical temperatures $u(x,t)$, for Example 2, with $\beta_1 = 0$ and (a) $\beta_2 = 0$, (b) $\beta_2 = 10^{-3}$, (c) $\beta_2 = 10^{-2}$, and (d) $\beta_2 = 10^{-1}$, with $p = 2\%$ noise. The relative error between them is also included.

5.3 Example 3 (for inverse problem II)

We consider now the inverse problem II given by equations (2)–(5) and (8) with the following input data:

$$\phi(x) = u(x,0) = x+1, \quad \mu_1(t) = u(0,t) = \frac{1}{1+t}, \quad \mu_2(t) = u(1,t) = \frac{2}{1+t},$$
$$\mu_3(t) = -a(t)u_x(0,t) = -1, \quad \psi(x) = \int_0^1 a(t)u(x,t)dt = x+1,$$
$$f(x,t) = (x+1)(2-x) - \frac{x+1}{(1+t)^2}.$$

One can observe that the conditions of Theorems 3 and 4 are satisfied, hence the problem is uniquely solvable. The analytical solution is given by

$$a(t) = 1+t, \quad c(x) = 2-x, \quad u(x,t) = \frac{x+1}{1+t}. \tag{40}$$

The initial guess was $\underline{a}^0 = \underline{1}$ and $\underline{c}^0 = \underline{2}$.

The above example was mentioned in [12, p.176]. We start the investigation of finding the unknown coefficients $a(t)$, $c(x)$ and the temperature $u(x,t)$ without noise in input data (4) and (5). Figure 13 shows the objective function (29), as a function of the number of iterations. From this figure it can be seen that a monotonic decreasing convergence is achieved in 193 iterations to reach a very low prescribed tolerance of $O(10^{-21})$.

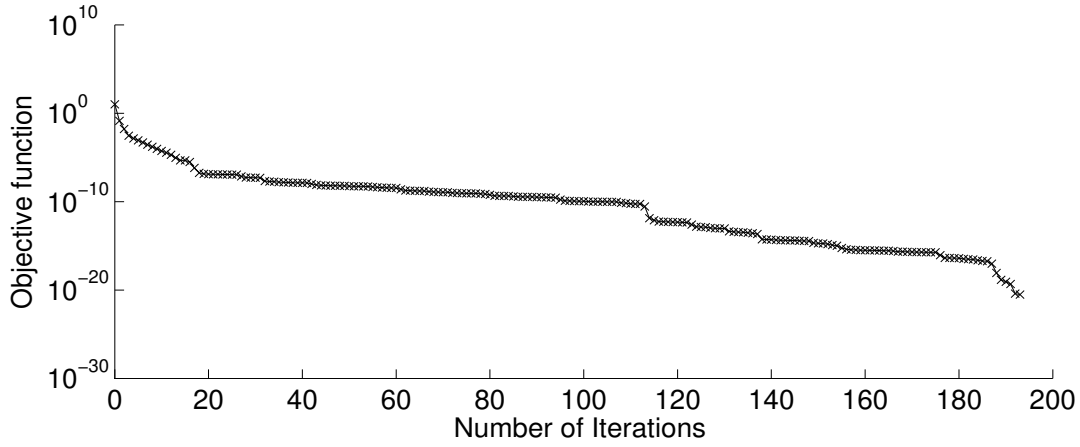

Figure 13: Objective function (29), for Example 3 with no noise and no regularization.

Figure 14 shows the numerical results for the associated time-dependent coefficient $a(t)$ and space-dependent coefficient $c(x)$ with no noise and no regularization. From this figure one can easily notice that there is an excellent agreement between the numerical and the exact solutions with $rmse(a)$=3.3E-4 and $rmse(c)$=1.1E-4.

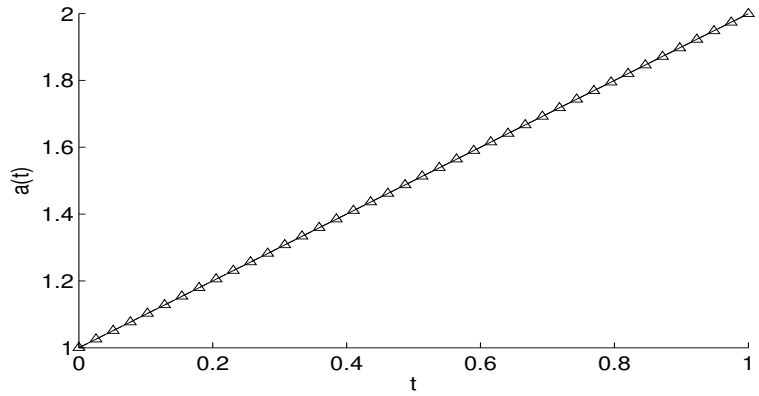

(a)

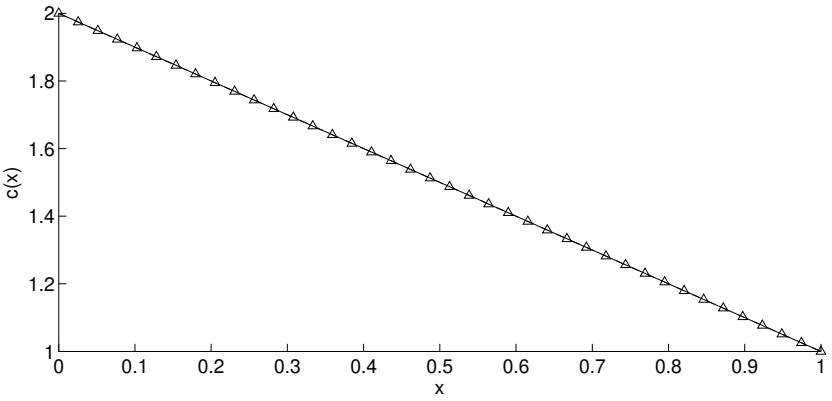

(b)

Figure 14: The exact (—) and numerical ($\triangle\triangle\triangle$) coefficients (a) $a(t)$, and (b) $c(x)$ for Example 3 with no noise and no regularization, obtained with $M = N = 40$.

Next, we investigate the stability of the solution with respect to noise. We include $p = 2\%$ additive Gaussian noise generated by equation (34). The input noisy data is therefore simulated numerically, via equation (30) for $\mu_3(t)$ and (32) for $\psi(x)$. Figure 15 shows the objective function (29), as a function of the number of iterations for various values of the regularization parameters. From this figure it can be seen that a monotonic decreasing convergence is achieved. Figure 16 shows the reconstructions of the coefficients $a(t)$ and $c(x)$. From this figure it can be seen that a very good estimation for $a(t)$ is obtained and less accurate for $c(x)$. Furthermore, one can be noticed that the coefficient $a(t)$ does not need to be regularized, i.e. we can take $\beta_1 = 0$ in (29). The $rmse$ (35) and (37), as well as other details, are included in Table 5.

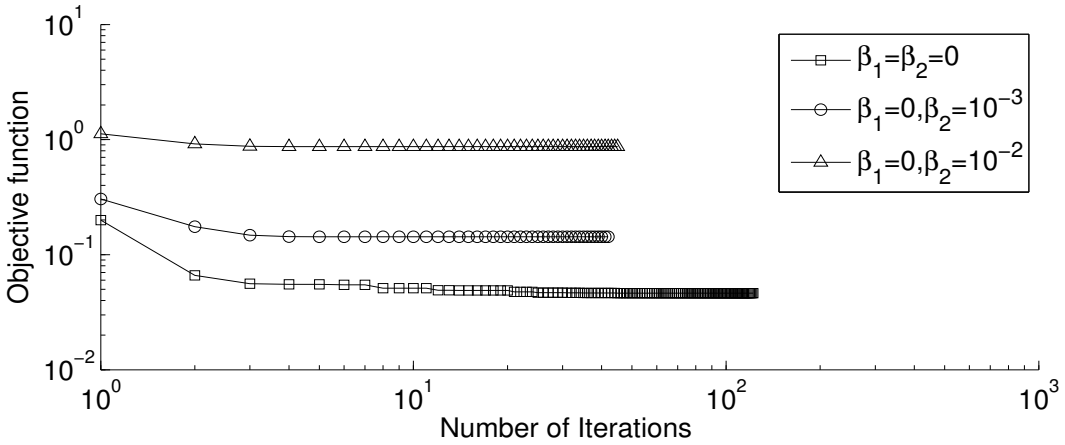

Figure 15: Objective function (29), for Example 3 with $p = 2\%$ noise and regularization.

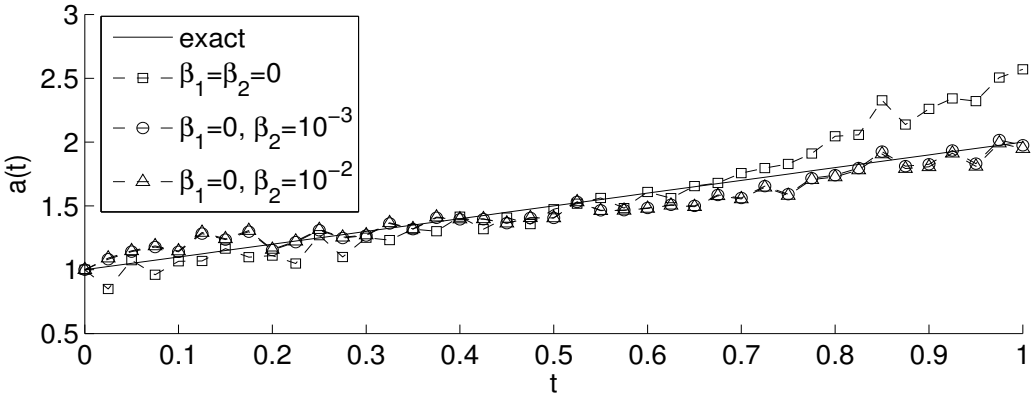

(a)

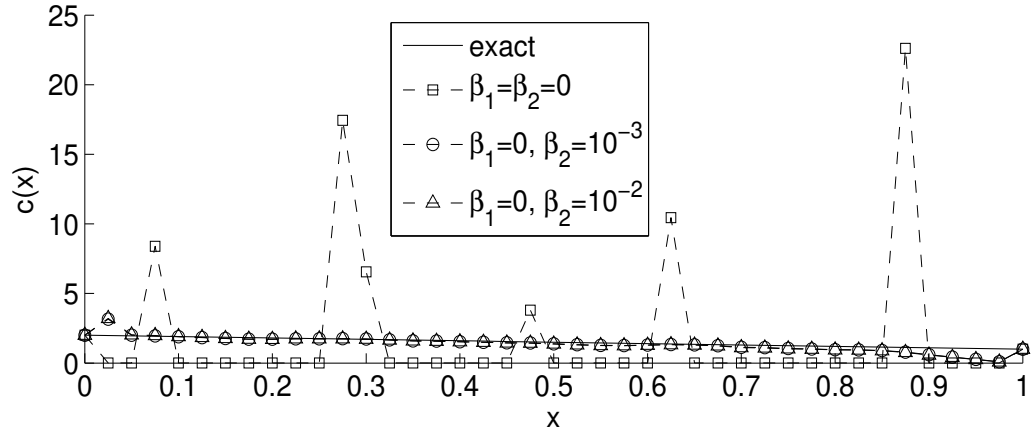

(b)

Figure 16: The coefficients (a) $a(t)$, and (b) $c(x)$ for Example 3 with $p = 2\%$ noise and regularization.

Figure 17 shows the exact and numerical solutions for the temperature $u(x, t)$ and the relative error between them. From this figure it can be seen that the numerical solution is stable and furthermore, its accuracy is consistent with the amount of noise included into the input data (4) and (5).

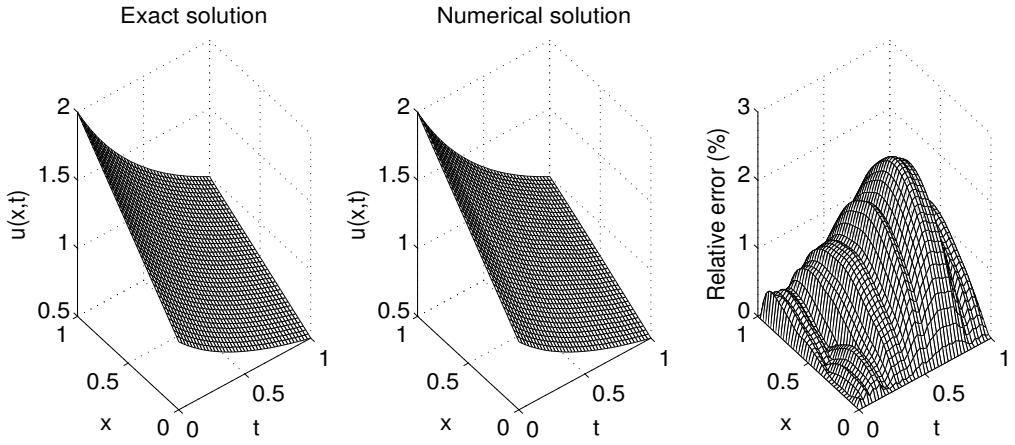

(a)

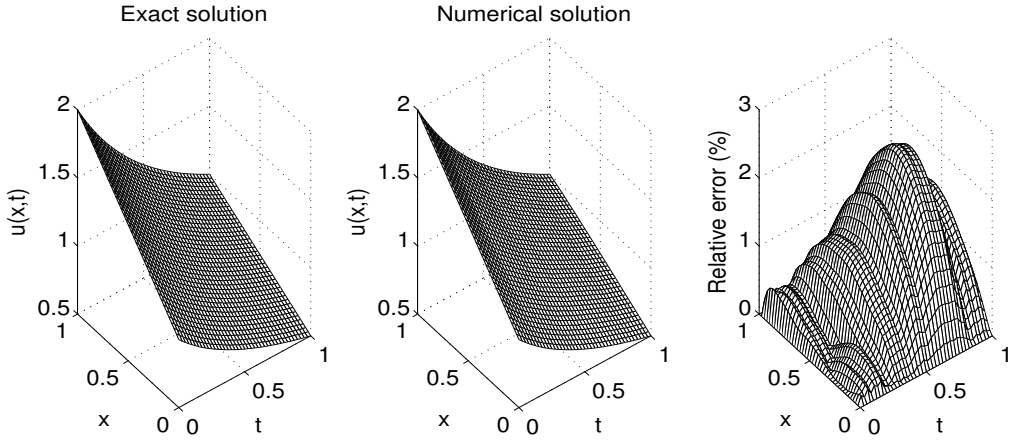

(b)

Figure 17: The exact and numerical temperature $u(x,t)$, for Example 3, with $\beta_1 = 0$ and (a) $\beta_2 = 10^{-3}$, and (b) $\beta_2 = 10^{-2}$, with $p = 2\%$ noise. The relative error between them is also included.

Table 5: Number of iterations, number of function evaluations, value of regularized objective function (29) at final iteration and the *rmse* values (35) and (37), for Example 3 with $p = 2\%$ noise.

$\beta_1 = 0$	$\beta_2 = 0$	$\beta_2 = 10^{-3}$	$\beta_2 = 10^{-2}$
No. of iterations	123	43	45
No. of function evaluations	10086	3526	3818
Minimum value of (29)	0.0463	0.1432	0.8684
$rmse(a)$	0.1705	0.0747	0.1761
$rmse(c)$	4.3624	0.3040	0.4554

5.4 Example 4 (for inverse problem II)

We now consider another test example for the inverse problem II given by equations (2)–(5) and (8), where the unknown coefficients $a(t)$ and $c(x)$ are not linear, with the following

input data:

$$\phi(x) = u(x,0) = e^x, \quad \mu_1(t) = u(0,t) = e^t, \quad \mu_2(t) = u(1,t) = e^{1+t},$$
$$\mu_3(t) = -a(t)u_x(0,t) = -(1+t^2)e^t, \quad \psi(x) = \int_0^1 a(t)u(x,t)dt = 2e^{1+x} - 3e^x,$$
$$f(x,t) = e^{x+t}(1-(1+t^2)(1-x^2)).$$

The condition of Theorem 4 are satisfied, hence the inverse problem has a unique solution. The analytical solution is given by

$$a(t) = 1 + t^2, \quad c(x) = x^2, \quad u(x,t) = e^{x+t}. \tag{41}$$

The initial guess was $\underline{a}^0 = \underline{1}$ and $\underline{c}^0 = \underline{0}$.

First we study the case of exact input data (4) and (5). The objective function (29) is plotted in Figure 18, as a function of the number of iterations. From this figure it can be seen that a nonsmooth decreasing convergence is obtained which levels to a stationary level of $O(10^{-9})$ in 302 iterations. The numerical results for the corresponding coefficients $a(t)$ and $c(x)$ are presented in Figure 19, and one can observe that the identified coefficients are in very good agreement with the exact ones in the absence of noise.

Next, we investigate the case of $p = 2\%$ noisy input data (4) and (5). The residual function (29) is plotted, as a function of number of iterations, in Figure 20 and a decreasing convergence can be observed. The corresponding coefficients are displayed in Figure 21 and good approximations are obtained for $a(t)$, but for $c(x)$ the numerical solution overshoots at various points and is unstable because no regularization has been employed yet.

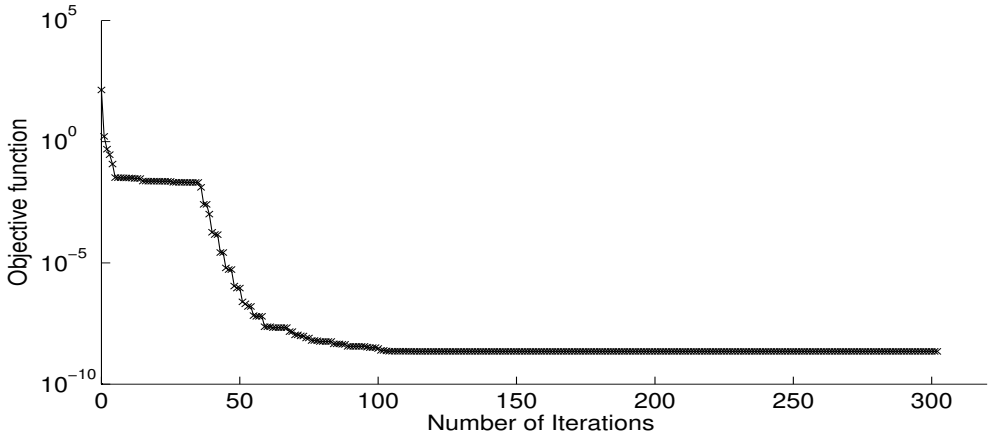

Figure 18: Objective function (29), for Example 4 with no noise and no regularization.

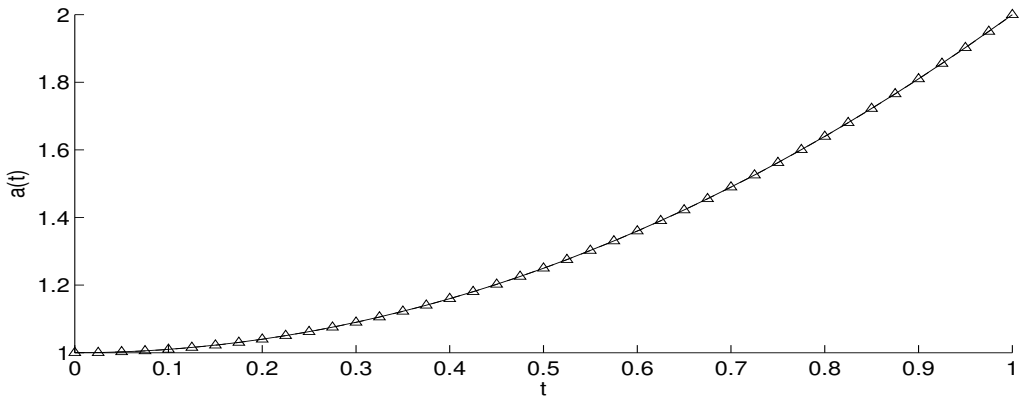

(a)

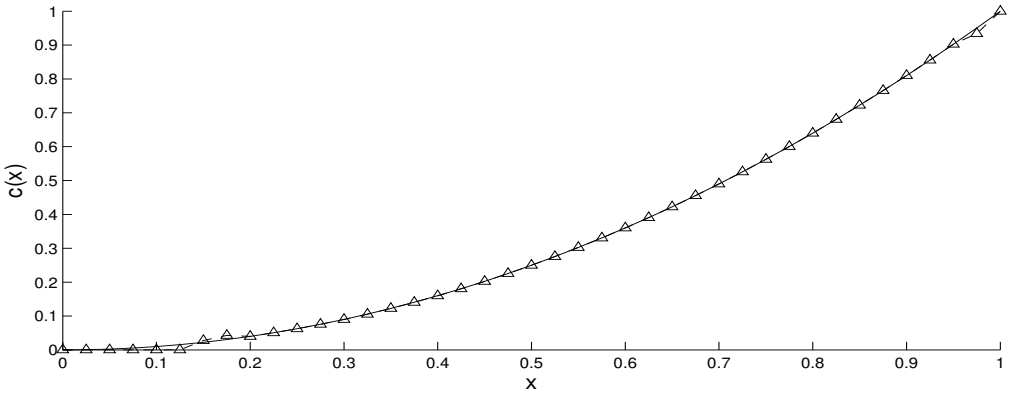

(b)

Figure 19: The exact (—) and numerical ($\triangle\triangle\triangle$) coefficients (a) $a(t)$, and (b) $c(x)$ for Example 4 with no noise and no regularization.

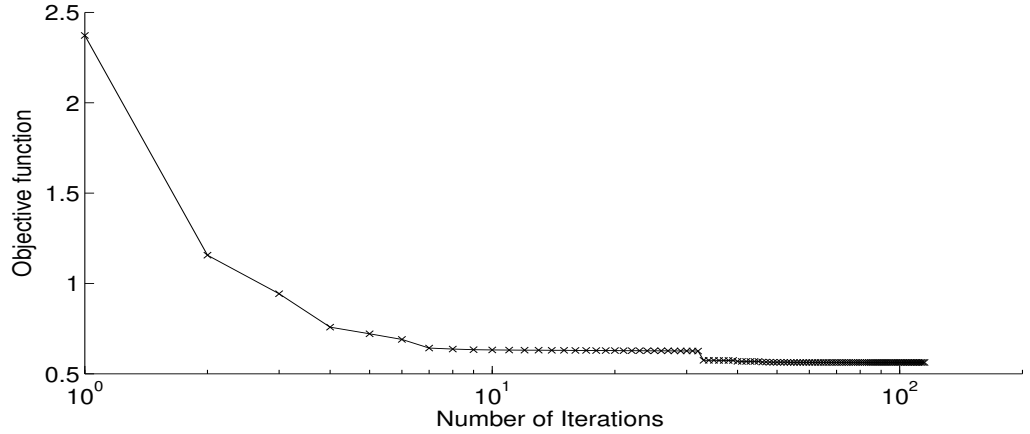

Figure 20: Objective function (29), for Example 4 with $p = 2\%$ noise and no regularization.

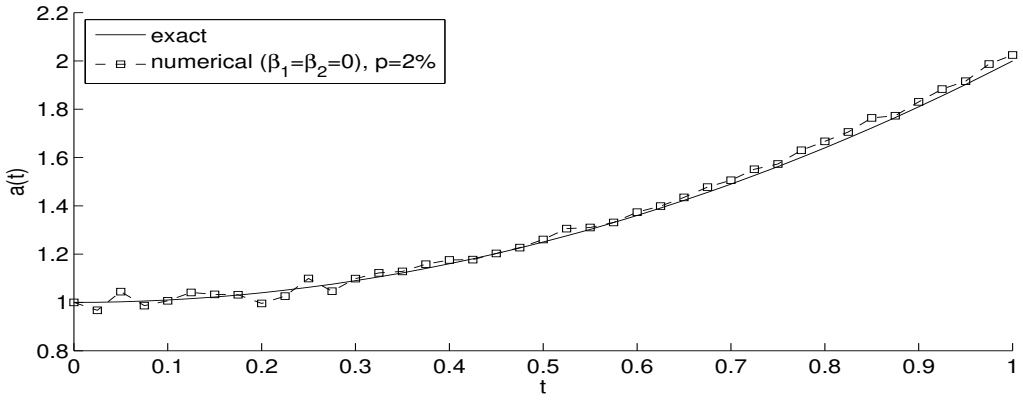

(a)

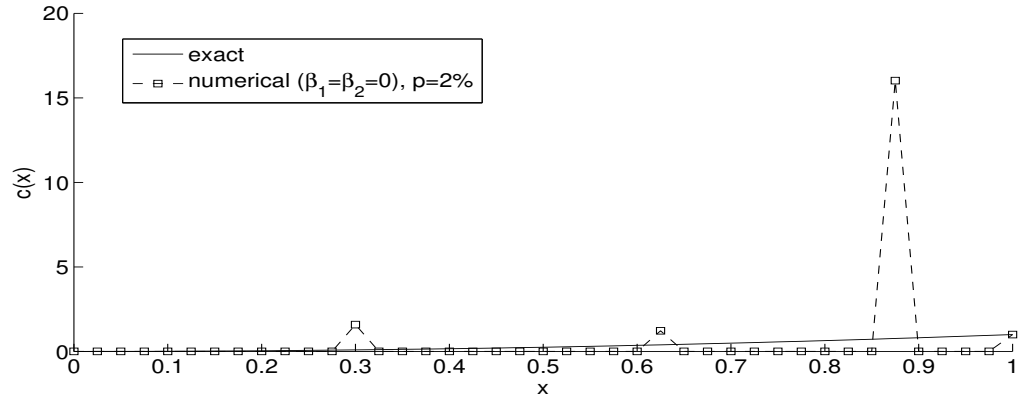

(b)

Figure 21: The coefficients (a) $a(t)$, and (b) $c(x)$ for Example 4 with $p = 2\%$ noise and no regularization.

As shown in Figure 21 the coefficient $a(t)$ seems rather stable. Therefore, we fix the value of β_1 to be zero and apply the regularization to the last term of objective function (29) for various values of the regularization parameter $\beta_2 \in \{10^{-3}, 10^{-2}, 10^{-1}\}$. Figure 22 shows the decreasing convergence of the objective function (29), as a function of the number of iterations. Figure 23 shows the retrieved coefficients for various values of β_2, and one can observe that the most accurate solution is obtained for $\beta_2 = 10^{-2}$, see also Table 6. In addition, as expected, the numerical solution for the temperature $u(x, t)$ is accurate, and stable, as illustrated in Figure 24.

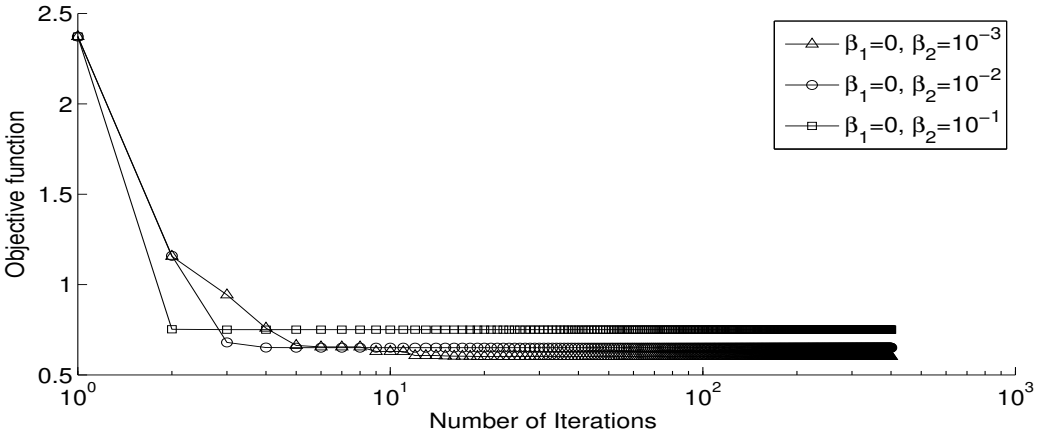

Figure 22: Objective function (29), for Example 4 with $p = 2\%$ noise and regularization.

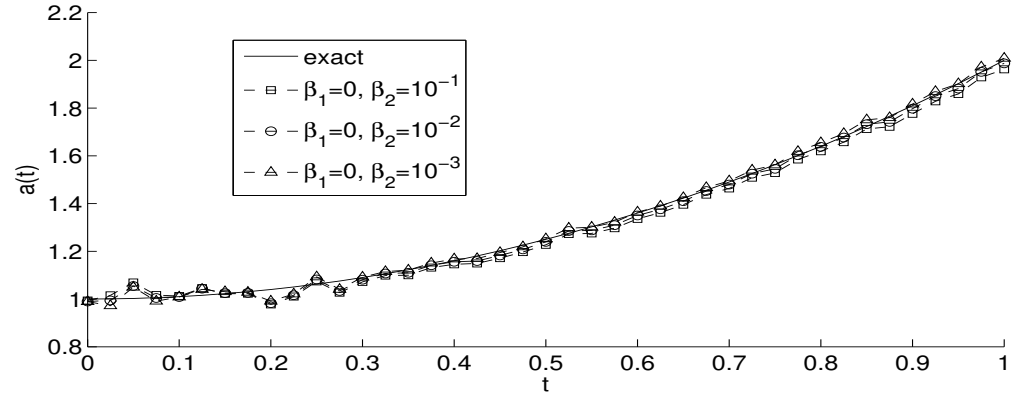

(a)

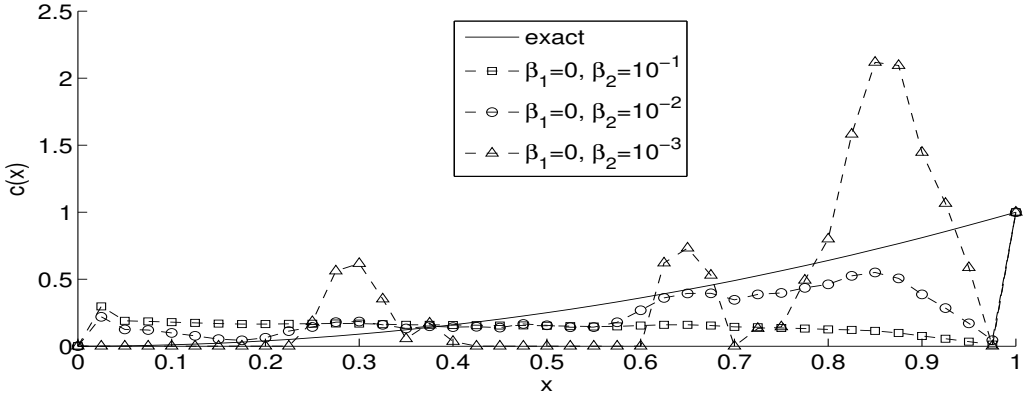

(b)

Figure 23: The coefficients (a) $a(t)$, and (b) $c(x)$ for Example 4 with $p = 2\%$ noise and regularization.

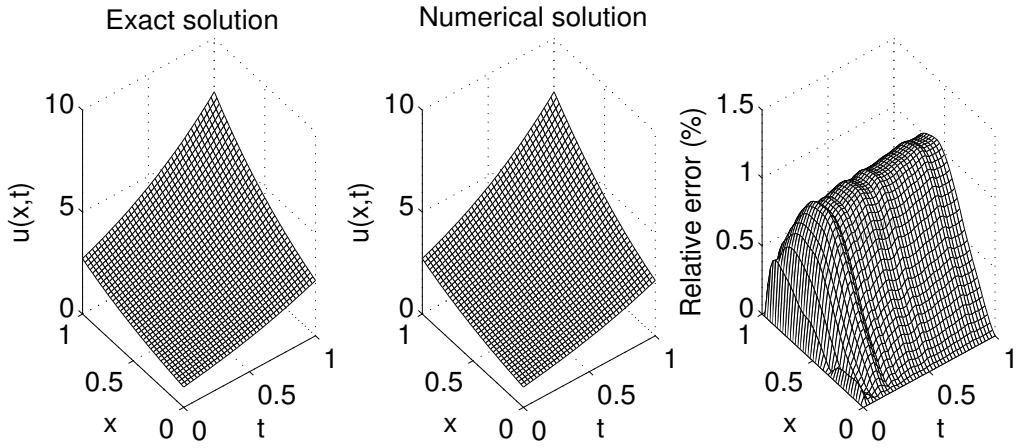

Figure 24: The exact and numerical temperatures $u(x,t)$, for Example 4, for $\beta_1 = 0$ and $\beta_2 = 10^{-2}$, with $p = 2\%$ noise. The relative error between them is also included.

Table 6: Number of iterations, number of function evaluations, value of regularized objective function (29) at final iteration and the *rmse* values (35) and (37), for Example 4 with $p = 2\%$ noise.

$\beta_1 = 0$	$\beta_2 = 10^{-3}$	$\beta_2 = 10^{-2}$	$\beta_2 = 10^{-1}$
No. of iterations	401	401	401
No. of function evaluations	33366	33366	33366
Minimum value of (29)	0.6023	0.6503	0.7501
$rmse(a)$	0.0181	0.0210	0.0313
$rmse(c)$	0.4498	0.2653	0.3848

6 Conclusions

This paper has presented a numerical approach to identify simultaneously the time and space-dependent coefficients together with the temperature in a parabolic heat equation. The additional conditions which ensure a unique solution are given by the heat flux measurement (4) and the total potential heat function specification (5) or, the time-average heat flux (6). The direct solver based on a Crank-Nicolson finite difference scheme was employed. The resulting inverse problems have been reformulated as constrained regularized minimization problems which were solved using the MATLAB optimization toolbox routine *lsqnonlin*. The inverse problems have been found rather stable in the time-dependent thermal conductivity coefficient $a(t)$, but less stable in the space-dependent coefficient $b(x)$ or $c(x)$. Numerical results obtained for a wide range of typical test examples showed that accurate and stable numerical solutions have been achieved. Possible future work may consist of extending the analysis to the reconstruction of higher dimensional space-dependent coefficients.

Acknowledgments

M.S. Hussein would like to thank the Higher Committee of Education Development in Iraq (HCEDiraq) for their financial support in this research. Enlighting discussions with Professor M. Ivanchov on Theorems 1–4 are gratefully acknowledged.

References

[1] L. Beilina and M.V. Klibanov, Approximate Global Convergence and Adaptivity for Coefficient Inverse Problems, Springer, Berlin, 2012.

[2] Z. Deng, J. Yu, L. Yang, Identifying the coefficient of first-order in parabolic equation from final measurement data, Math. Comput. Simul. 77 (2008) 421–435.

[3] H.W. Engl and P. Kugler, Nonlinear inverse problems: theoretical aspects and some industrial applications, In: Multidisciplinary Methods for Analysis, Optimization and Control of Complex Systems, (eds. V. Capasso and J. Priaux), Springer, Berlin, Vol. 6 of the series Mathematics in Industry, 2005, pp. 3-47.

[4] A. Erdem, D. Lesnic, A. Hasanov, Identification of a spacewise dependent heat source, Appl. Math. Model. 37 (2013) 10231–10244.

[5] A.G. Fatullayev, Numerical procedure for the determination of an unknown coefficient in parabolic equations, Comput. Phys. Commun. 144 (2002) 29–33.

[6] A. Fatullayev, S. Cula, An iterative procedure for determining an unknown spacewise-dependent coefficient in a parabolic equation, Appl. Math. Lett. 22 (2009) 1033–1037.

[7] A. Hazanee, D. Lesnic, Determination of a time-dependent heat source from nonlocal boundary conditions, Eng. Anal. Boundary Elements 37 (2013) 936–956.

[8] W. Hundsdorfer, J.G. Verwer, Numerical Solution of Time-Dependent Advection-Diffusion-Reaction Equations, Springer Series in Computational Mathematics, Berlin, 2003.

[9] M.I. Ivanchov, Inverse problem of finding a major coefficient in a parabolic equation, Matematychi Studii 8 (1997) 214–220.

[10] M.I. Ivanchov, Détermination simultanée de deux coefficients aux variables diverses dans une équation parabolique, Matematychi Studii 10 (1998) 173–187.

[11] M.I. Ivanchov, Inverse problem of simultaneous determination of two coefficients in a parabolic equation, Ukrainian Math. J. 52 (2000) 379–387.

[12] M.I. Ivanchov, Inverse Problems for Equations of Parabolic Type, VNTL Publications, Lviv, Ukraine, 2003.

[13] A. Joshi, W. Bangerth and E. Sevick-Muraca, Adaptive finite element based tomography for fluorescence optical imaging in tissue, Optics Express 12 (2004) 5402–5417.

[14] V.L. Kamynin, Inverse problem of finding the coefficient of a lower derivative in a parabolic equation on the plane, Diff. Eqns. 48 (2012) 214–223.

[15] V.L. Kamynin, The inverse problem of determining the lower-order coefficient in parabolic equations with integral observation, Math. Notes 94 (2013) 205–213.

[16] O.A. Ladyzenskaja, V.A. Solonnikov, N.N. Uralceva, Linear and Quasi-linear Equations of Parabolic Type, Translations of Mathematical Monographs 23, Providence, R.I., American Mathematical Society, 1968.

[17] D. Lesnic, S.A. Yousefi, M. Ivanchov, Determination of a time-dependent diffusivity from nonlocal conditions, J. Appl. Math. Computing 41 (2013) 301–320.

[18] Mathworks R2012 Documentation Optimization Toolbox-Least Squares (Model Fitting) Algorithms, available from www.mathworks.com/help/toolbox/optim/ug /brnoybu.html.

[19] D.A. Murio, The Mollification Method and the Numerical Solution of Ill-Posed Problems, Wiley, New York, 1993.

[20] K. Parand, J.R. Rad, Kansa method for the solution of a parabolic equation with an unknown spacewise-dependent coefficient subject to an extra measurement, Computer Phys. Commun. 184 (2012) 582–595.

[21] A. Rhoden, N. Patong, Y. Liu, J. Su and H. Liu, A globally convergent numerical method for coefficient inverse problems with time-dependent data, Springer Proceedings in Mathematics & Statistics 48 (2013) 105–128.

[22] M. Slodicka, Determination of a solely time-dependent source in a semilinear parabolic problem by means of boundary measurements, J. Comput. Appl. Math. 289 (2015) 433–440.

[23] G.D. Smith, Numerical Solution of Partial Differential Equations: Finite Difference Methods, third ed., Oxford Applied Mathematics and Computing Science Series, 1985.

[24] A.N. Tikhonov, A. Goncharsky, V. Stepanov, A.G. Yagola, Numerical Methods for the Solution of Ill-Posed Problems, Kluwer Academic Publishers, Dordrecht, 1995.

[25] D. Trucu, D.B. Ingham, D. Lesnic, Space-dependent perfusion coefficient identification in the transient bio-heat equation, J. Eng. Math. 67 (2010) 307–315.

[26] K. Van Bockstal and M. Slodicka, Determination of an unknown diffusion coefficient in a semilinear parabolic problem, J. Comput. Appl. Math. 246 (2013) 104–112.

[27] C.R. Vogel, Computational Methods for Inverse Problems, SIAM, Philadelphia, 2002.